Atmospheric Moisture Transport to the Arctic: Assessment of Reanalyses and Analysis of Transport Components

Ambroise Dufour, Olga Zolina, Sergei K. Gulev

Atmospheric Moisture Transport to the Arctic: Assessment of Reanalyses and Analysis of Transport Components

AMBROISE DUFOUR

LGGE, CNRS/UJF, Grenoble, France

OLGA ZOLINA

LGGE, CNRS/UJF, Grenoble, France, and P. P. Shirshov Institute of Oceanology, Moscow, Russia

SERGEY K. GULEV

P. P. Shirshov Institute of Oceanology, Moscow, Russia

(Manuscript received 10 August 2015, in final form 1 April 2016)

ABSTRACT

The atmospheric water cycle of the Arctic is evaluated via seven global reanalyses and in radiosonde observations covering the 1979–2013 period. In the regional moisture budget, evaporation and precipitation are the least consistent terms among different datasets. Despite the assimilation of radiosoundings, the reanalyses present a tendency to overestimate the moisture transport. Aside from this overestimation, the reanalyses exhibit a remarkable agreement with the radiosondes in terms of spatial and temporal patterns. The northern North Atlantic, subpolar North Pacific, and Labrador Sea stand out as the main gateways for moisture to the Arctic in all reanalyses. Because these regions correspond to the end of the storm tracks, the link between moisture transports and extratropical cyclones is further investigated by decomposing the moisture fluxes in the mean flow and transient eddy parts. In all reanalyses, the former term tends to cancel out when averaged over a latitude circle, leaving the latter to provide the bulk of the midlatitude moisture imports (89%–94% at 70°N). Although the Arctic warms faster than the rest of the world, the impact of these changes on its water cycle remains ambiguous. In most datasets, evaporation, precipitation, and precipitable water increase in line with what is expected from a warming signal. At the same time, the moisture transports have decreased in all the reanalyses but not in the radiosonde observations, though none of these trends is statistically significant. The fluxes do not scale with the Clausius–Clapeyron relation because the increasing humidity is not correlated with the meridional wind, particularly near the surface.

1. Introduction

The observed Arctic climate variability is characterized by strong warming with a surface temperature trend twice as large as the global trend during the last few decades (Polyakov et al. 2002; Serreze et al. 2009; Screen and Simmonds 2010; Hartmann et al. 2013). The sea ice extent in September has declined at a rate of 12.4% decade^{-1} from 1979 to 2010 with an associated reduction in ice thickness (Stroeve et al. 2012). The results from phase 5 of the Coupled Model Intercomparison Project (CMIP5) indicate that these tendencies will continue during the twenty-first century under different emission scenarios (Collins et al. 2013).

Both the decrease in sea ice and increase in temperatures are expected to intensify the regional hydrological cycle by increasing evaporation and the water-holding capacity of the air. The intensification of the atmospheric water cycle may be driven by local evaporation over ice-free oceans (Bintanja and Selten 2014; Kopec et al. 2016) or by stronger moisture advection from subpolar and midlatitudes (Bengtsson et al. 2011; Zhang et al. 2013). Changes in the water cycle would have various consequences. Precipitation variability plays an important role in forming the Arctic Ocean freshwater budget (Serreze et al. 2006) and the surface mass balance of the Greenland ice sheet (Ettema et al. 2009; Burgess

Corresponding author address: Ambroise Dufour, Laboratoire de Glaciologie et Géophysique de l'Environnement, 54 rue Molière, BP 96, F-38402 Saint-Martin d'Hères CEDEX, France.
E-mail: ambroise.dufour@gmail.com

DOI: 10.1175/JCLI-D-15-0559.1

et al. 2010). Furthermore, the availability of moisture controls the formation of clouds, which impact the surface energy budget, particularly in winter when longwave downwelling radiation dominates (Woods et al. 2013). Through the direct radiative impact and indirect effect on clouds, increasing amounts of moisture then feed back onto the surface warming.

In situ observations of the components of the hydrological cycle are rare in the Arctic, particularly over the ocean. The sparse terrestrial station network (relative to the midlatitudes), buoys, drifting ice stations, and occasional scientific cruises do not provide adequate temporal and spatial coverage for an explicit description of the regional climate and its evolution. Satellite data are indirect and subject to large uncertainties and may be limited in time by several years for specific instruments (Groves and Francis 2002; Boisvert et al. 2013). Atmospheric reanalyses benefit from both in situ and remote sensing observations and likely constitute the most comprehensive source of information on the Arctic hydrological budget at present. However, neither precipitation nor evaporation is assimilated in global reanalyses; instead, they are computed based on model physics during the generation of the first-guess field. As a result, these variables vary considerably across the reanalyses; for instance, the net precipitation (precipitation minus evaporation) over global land areas varies by a factor of 2 between NCEP–NCAR R1 and NCEP CFSR (Trenberth et al. 2011). Moisture transport, however, is computed from wind and humidity, both of which are analyzed; hence, the results are more consistent among datasets. Trenberth et al. (2011) reported only a 43% difference in moisture convergence over land between NCEP–NCAR R1 and NCEP CFSR. For the Arctic, the difference between the moisture transport estimated by ERA-40 (Jakobson and Vihma 2010) and MERRA (Cullather and Bosilovich 2011) is below 10%. Transport-based estimates of convergences also tend to be less affected by changes in the observation system unlike precipitation and evaporation. In MERRA, for example, the transition from TOVS to ATOVS between 1998 and 2001 introduced a positive trend in global precipitation that is absent from the observational records (Trenberth et al. 2011).

Our work builds upon a number of previous studies evaluating moisture transport in reanalyses, starting with Cullather et al. (2000) on NCEP–NCAR R1 and ERA-15. Groves and Francis (2002) are noteworthy for having decomposed the moisture flux into the monthly mean flow and transient eddy contributions demonstrating the predominance of the latter, confirming the results of Peixoto and Oort (1992). More recently, Cullather and Bosilovich (2011) analyzed the Arctic moisture budget as depicted in MERRA and included comparisons of evaporation and precipitation fields from ERA-Interim and CFSR. We extend the comparison to JRA-55 as well as the older reanalyses—NCEP–NCAR R1, NCEP–DOE R2, and JRA-25—all of which been continued up to 2013 (unlike ERA-40). Besides evaporation and precipitation, we specifically focus on water vapor advection, as it is more stable and better suited to establish model-independent features of the hydrological cycle variability. This variable can also be validated against observations—namely, radiosonde data. Besides a characterization of mean climatology, seasonal cycle, and interannual variability, we perform a decomposition similar to Peixoto and Oort (1992) to gain further insight into the mechanisms responsible for transporting moisture to the high northern latitudes.

The remainder of this paper is organized as follows. Section 2 briefly describes the data sources—namely, seven reanalyses and radiosoundings—and section 3 presents the methods used to compute moisture transports. The results presented in section 4 are subdivided into the analysis of the climatological spatial structure, of long-term moisture budgets, of the transport components due to the mean flow and transient eddies, and of the seasonal cycle and interannual variability of the source terms in the different reanalyses. Section 5 summarizes the results, discusses the reliability of our estimates of the variability in water vapor transport, and suggests some directions for future research.

2. Data

a. Reanalyses

Reanalyses, or retrospective analyses, provide a dynamically consistent view of the past state of the atmosphere by optimally combining numerical weather forecasts with historical atmospheric observations. The forecast models and data assimilation schemes are frozen, but the input streams may change during the reanalysis period. Consequently, a trend or shift in the reanalysis data may reflect a modification in the observing system rather than a climatic phenomenon; trends derived from reanalysis data should be treated with caution (Bengtsson et al. 2004a). This is particularly important for the Arctic, where the assimilation relies predominantly on satellite data.

We use outputs from seven reanalyses (Table 1): NCEP–NCAR R1 (Kalnay et al. 1996), NCEP–DOE R2 (Kanamitsu et al. 2002), JRA-25 (Onogi et al. 2007), ERA-Interim (Dee et al. 2011), NCEP CFSR (Saha et al. 2010), MERRA (Bosilovich et al. 2006; Rienecker et al. 2011), and JRA-55 (Ebita et al. 2011; Kobayashi

TABLE 1. Major characteristics of reanalyses compared during the study.

Reanalysis	Model vintage	Model resolution	Available resolution	Data assimilation
NCEP–NCAR R1	1995	T62 L28	2.5° L8	3D-Var
NCEP–DOE R2	2001	T62 L28	2.5° L10	3D-Var
JRA-25	2004	T106 L40	1.25° L10	3D-Var
ERA-Interim	2006	T255 L60	0.75° L23	4D-Var
NCEP CSFR	2009	T382 L64	0.5° L23	3D-Var + FOTO
MERRA	2009	1/2° × 2/3° L72	1/2° × 2/3° L23	3D-Var + IAU
JRA-55	2009	T319 L60	0.5° L23	4D-Var

et al. 2015). In addition to the increasing spatial resolution—from T62 in NCEP R1 to T382 in CFSR—the modern reanalyses distinguish themselves from the first generation by their improved model physics and data assimilation systems, particularly regarding satellite observations. ERA-Interim and JRA-55 both implement four-dimensional variational data assimilation (4D-Var) to account for the observations' temporal distribution within the assimilation window. Unlike the other datasets, MERRA is based on finite volume dynamics. Its incremental analysis update (IAU) scheme improves upon 3D-Var by dampening the analysis increment. In IAU, a correction is applied to the forecast model gradually, limiting precipitation spinup in particular. CFSR still relies on 3D-Var but with a refinement—first-order time interpolation to the observation (FOTO; Rančić et al. 2008). CFSR also couples atmosphere, simplified ocean, and sea ice models to generate the 6-hourly guess field.

The moisture budget of an atmospheric column can be analyzed by evaluating either side of the moisture balance equation:

$$\frac{\partial}{\partial t}\int_0^{p_s} q\frac{dp}{g} + (P - E) = -\text{div}\int_0^{p_s} q\mathbf{V}\frac{dp}{g}, \qquad (1)$$

where q is specific humidity, g the standard gravity, p the pressure vertical coordinate, $\mathbf{V}$ the wind, E evaporation, P precipitation, and p_s the surface pressure. The first term on the right-hand side, the precipitable water tendency, is typically negligible compared to the other terms for yearly time scales. The second term, $(P - E)$, or net precipitation, is computed by accumulating precipitation and evaporation during the generation of the model first guess. This is the so-called physics output method. NCEP–NCAR R1, NCEP–DOE R2, JRA-25, and NCEP CFSR do not provide a ready-made evaporation product; thus, we computed it from the latent heat flux using the skin temperature and snow and ice cover to determine the phase-change enthalpy. The second method, referred to as the "aerological" method, evaluates the right-hand side of Eq. (1), the moisture flux convergence, which is based on analyzed humidity and winds. The two methods yield different results; thus, the moisture budget of the reanalyses is typically not closed (e.g., Trenberth et al. 2011; Cullather and Bosilovich 2011). The physics output method is more dependent on model physics and tends to be affected by changes in input data streams. The aerological method is more stable, and its output in different reanalyses is more coherent (Trenberth et al. 2011).

b. *In situ observations*

To validate the characteristics of moisture transport derived from reanalyses, we compared them to observations—namely, radiosoundings from the integrated global radiosonde archive (IGRA; Durre et al. 2006). For the region north of 60°N, 74 sites were active throughout the satellite era from 1979 to 2013 (Fig. 1). Of these, 39 sites are located on the coast, including 6 on small islands. The observation frequency ranges from once to twice daily and corresponds to the synoptic times used in operational and retrospective analyses. Measurements are supposed to be available at least on certain standard levels, which are 1000, 850, 700, 500, 400, 300, 250, and 200 hPa in the troposphere.

IGRA does not constitute independent data; finding radiosoundings that are not assimilated in reanalyses is quite a challenge (Francis 2002). Nevertheless, radiosoundings are important to check the internal consistency of the data assimilation schemes. There may be conflicts between in situ and remote sensing sources, as in Grant et al. (2008), or the observations may be overridden by the model. Radiosoundings also have their limitations particularly at low humidity levels. In certain cases, the assimilation procedure may be justified in giving them little weight.

Before being archived in IGRA, soundings pass a number of quality control checks. The pressure, temperature, and geopotential height variables receive particular attention. However, the specific humidity and winds, which are of special interest to us, did not undergo climatological checks in IGRA; thus, we performed additional quality screens on these variables to filter out extremely high values. For this purpose, we used the median as an indicator of central tendency and

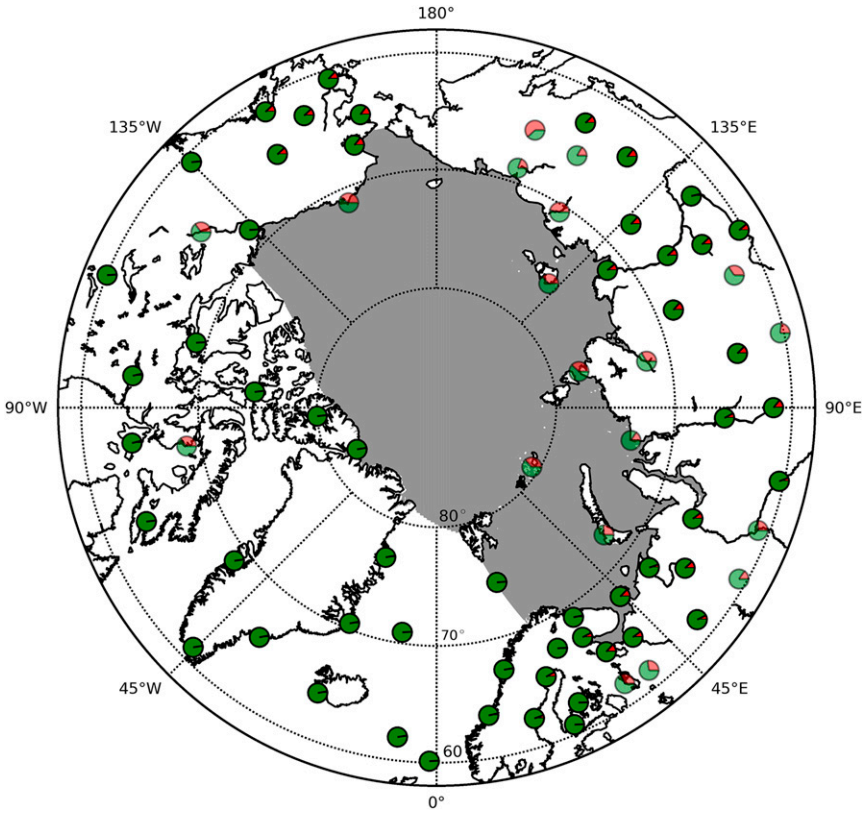

FIG. 1. Radiosonde launch sites active from 1979 to 2013 (green circles) with the proportion of missing daily values shown in orange–red colors. Rejected sites are have lighter-green circles. The gray shading indicates the Arctic Ocean domain defined in Serreze et al. (2006).

the interquartile range (IQR) as a measure of spread. Means and standard deviations are overly sensitive to outliers and yield artificially high thresholds. We computed the medians and IQRs for each calendar month to account for the variability due to the annual cycle. After subjective examinations of unnatural shifts and outliers in the time series and vertical profiles, we chose to remove values lying outside the range of ±4 IQR from the median. Because the IQR of a Gaussian distribution is 1.35 times its standard deviation (σ), our criterion corresponds to approximately 5.4σ. Although this threshold seems permissive, it excludes 4.8% of the wind data and 5.5% of the humidity data. Additionally, we required the existence of values on at least five pressure levels before performing linear interpolations of the vertical profiles. Finally, we only considered stations with at least 85% of days with valid soundings over the entire period, which led us to discard 11 sites.

To avoid a sampling bias, we only compared simultaneous observations and reanalysis values. The collocation of reanalysis data with radiosonde sites was performed via bilinear interpolation. Before we averaged a variable over the radiosonde sites, we first grouped the stations in eight 45° longitudinal sectors. We averaged the variable within these longitudinal bands after which the averaging was applied over the bands. In this manner, the data-rich regions (such as Europe) are not given an unfair emphasis. We were also concerned that our filters would be biased against intense moisture events because they exclude exceptionally high values of humidity and wind. Table 2 shows that the mean meridional moisture fluxes in reanalyses over

TABLE 2. Mean meridional moisture flux averaged over all radiosonde sites in reanalyses and IGRA ($\mathrm{kg\,m^{-1}\,s^{-1}}$). The reanalyses were collocated in both time and space with the soundings in the middle column but only in space in the right column.

Dataset	Subsampled	Unsampled
NCEP–NCAR R1	9.31	10.04
NCEP–DOE R2	9.47	10.11
JRA-25	9.52	9.68
ERA-Interim	9.66	9.67
NCEP CFSR	9.33	9.48
MERRA	9.92	10.26
JRA-55	9.47	9.71
IGRA	8.76	

TABLE 3. Comparison of the various numerical methods to compute the time-averaged (1979–2013) moisture convergence in the polar caps north of 70°N and north of 60°N, the Arctic Ocean, and the Greenland ice sheet (mm yr^{-1}).

Region	Reanalysis	Pressure levels	Model levels	Convergence product
70°–90°N	ERA-Interim	195.8	194.7	194.4
	MERRA	200.6	202.3	
	JRA-55	193.2	190.7	
60°–90°N	ERA-Interim	258.2	257.4	256.6
	MERRA	258.3	265.9	
	JRA-55	261.7	260.6	
Arctic Ocean	ERA-Interim	184.9	184.5	184.5
	MERRA	217.7	226.3	
	JRA-55	185.5	185.5	
Greenland	ERA-Interim	177.6	177.7	177.1
	MERRA	389.9	395.3	
	JRA-55	157.7	155.2	

the radiosonde sites are only slightly reduced by the subsampling.

3. Methods

To calculate the moisture budget of a given region we integrated the moisture balance equation [Eq. (1)].

We followed Serreze et al.'s (2006) definition of the Arctic Ocean and Cullather and Bosilovich's (2011) definition of the Greenland ice sheet. We used finite differences to compute the divergence, which introduces an error, noted by Seager and Henderson (2013). ERA-Interim provides a vertically integrated moisture convergence product calculated in spectral space on model levels. Over Greenland, the value deviates by 0.3% from the finite differences result and is even smaller over the Arctic Ocean. When we computed the water budget over a polar cap (e.g., the region north of 70°N), the divergence term simplified to the following:

$$\iint_{\phi>70^\circ}\int_0^{p_s} \mathrm{div}(q\mathbf{V})\frac{dp}{g}\,ds = -\int_{-\pi}^{\pi}\int_0^{p_s} q\frac{dp}{g}\,d\lambda\,, \quad (2)$$

where ds is a surface element, ϕ is the latitude, and λ is the longitude.

Ideally, the numerical vertical integrations should be made on model levels. Unfortunately, for NCEP–NCAR R1, NCEP–DOE R2, NCEP CFSR, and JRA-25, we only had specific humidities and winds on pressure levels from $p_0 = 1000$ hPa to $p_N = 200$ hPa (300 hPa for NCEP–NCAR R1); above these levels, moisture concentrations become negligible. The value of the variable on the lowest pressure level above the ground was taken to be the value of the variable at the surface. Let p_{n_0} be that level. The vertical integral of any variable $f(p)$ was approximated following the trapezoidal rule:

$$\int_0^{p_s} f(p)\,dp \approx \sum_{n=n_0}^{N-1}\frac{1}{2}[f(p_{n+1})+f(p_n)](p_n-p_{n+1}) + f(p_{n_0})(p_s-p_{n_0}). \quad (3)$$

Fluxes on model levels were available for ERA-Interim, MERRA, and JRA-55 and could be compared with the pressure level estimates. In all four regions considered, the relative differences in mean moisture convergence were below 4% and as low as 2% for the polar cap north of 70°N. The effects of the various numerical approximations are summarized in Table 3.

To elucidate which time scales contribute most to the net moisture imports, we decompose the winds and humidity into mean and fluctuation (respectively denoted by overbars and primes) using monthly averages to filter the synoptic transients as in Peixoto and Oort (1992). For a given location and altitude, the mean moisture flux breaks down into two terms, one due to transient eddies, the other to the mean flow:

$$\overline{q\mathbf{v}} = \overline{q'\mathbf{v}'} + \overline{q}\,\overline{\mathbf{v}}. \quad (4)$$

Other applications of the Reynolds decomposition to the atmospheric moisture transport to the Arctic can be found in Groves and Francis (2002), Oshima and Yamazaki (2006), Newman et al. (2012), and Liu and Barnes (2015), on other individual datasets.

Following Peixoto and Oort (1992), we introduce additional notations to refer to the zonal mean $[q]$, the vertical mean on pressure levels $\{q\}$, and the deviations therefrom q° and q^*. After vertical and zonal averaging of the meridional flux, we further decompose the mean flow term:

$$\{[\overline{q}\overline{\mathbf{v}}]\} = \{[\overline{q'\mathbf{v}'}]\} + \{[\overline{q}^*\overline{\mathbf{v}}^*]\} + \{[\overline{q}]^\circ[\overline{\mathbf{v}}]^\circ\} + \{[\overline{q}]\}\{[\overline{\mathbf{v}}]\}. \quad (5)$$

The first term on the right-hand side groups the contribution of small-scale, short-lived, ''transient eddies,'' including extratropical cyclones. The second term is the product of the zonal anomalies of the mean humidity and wind fields which are designated as ''stationary eddies.'' For instance, in the North Atlantic at 70°N, the air is particularly moist and the meridional wind is particularly strong compared to other longitudes. The third term on the right-hand side corresponds to the product of vertical anomalies in the zonally symmetric time mean humidity and wind fields, known as ''vertical cells'' by reference to the overturning circulations of the Hadley, Ferrel, and polar cells. The fourth and last term should be zero because there is no net mass flux into a closed region on yearly time scales. We test this assumption in the following section.

Throughout this study, we used each reanalysis's output grid to perform all computations, including Reynolds decomposition, vertical integrations, and spatial averages. When necessary for the comparison and as the final stage, we bilinearly interpolated the derived products on a common grid (0.5° × 0.5° latitude–longitude).

4. Results

a. *Spatial structure of the Arctic moisture transport*

We now examine the Arctic atmospheric hydrological cycle as represented by the seven reanalyses studied, with an emphasis on moisture transport. Whenever possible, we compare the reanalyses to the radiosonde observations.

To the first order, the mean vertically integrated moisture fluxes north of 60°N in ERA-Interim follow an eastward zonally symmetric flow with magnitudes of approximately 25 $kg\,m^{-1}\,s^{-1}$ (Fig. 2a). The magnitudes decrease with latitude following the decreasing temperature and humidity, from 70 $kg\,m^{-1}\,s^{-1}$ over northern Europe to zero over the central Arctic. Deviations occur from the zonal pattern, particularly in the northern North Atlantic as shown in Fig. 2b. Transport over the Denmark Strait is clearly influenced by the cyclonic circulation associated with the Icelandic low. Over the Norwegian Sea, the transport is the most intense (more than 80 $kg\,m^{-1}\,s^{-1}$) and exhibits a definite northward component. Over Alaska and the Bering Strait, the transport is weaker in magnitude (approximately 50 $kg\,m^{-1}\,s^{-1}$) but is directed straight toward the North Pole; the same holds for the Labrador Sea and the Davis Strait.

The other datasets correspond well with the broad features of this climatology. As shown in Fig. 2c, the differences between the mean moisture transport in ERA-Interim and in the other reanalyses are on the order of 10 $kg\,m^{-1}\,s^{-1}$, constituting approximately one-fifth to one-fourth of the mean transport magnitude. The differences in model resolution are likely the reason for the larger spread over regions with complex orography such as Alaska, Scandinavia, and Greenland. The first-generation datasets, NCEP–NCAR R1 and NCEP–DOE R2 (turquoise and orange arrows in Figs. 2c,d), are often in disagreement with the other reanalyses in these areas. Their relatively coarse resolution (T62, 2.5°) does not allow finescale features, such as those off the southwestern shore of Greenland, to be adequately captured. In the higher-resolution versions of Fig. 2 (not shown here), the ensemble spread was not appreciably reduced in the vicinity of the radiosonde sites.

The longitude distribution of moisture transports at 70°N confirms the consensus among different reanalyses (Fig. 3). No dataset shows systematically lower or higher climatological moisture transport. The differences across products are within the range of interannual variability, except for the above-mentioned regions of large disagreement. There, the longitude profiles of the modern reanalyses reflect the rugged relief beneath which the first-generation datasets smooth out.

To evaluate the reliability of the moisture transport estimates in the reanalyses, we compared them to the IGRA radiosonde observations described in section 2. Considering climatological fluxes, the observed longitudinal pattern is broadly respected by the reanalyses (Fig. 4a). Aside from two outliers (Petchora station in the northern Ural Mountains and Narsarsuaq station in Greenland), correlations between moisture flux monthly anomalies in reanalyses and radiosoundings are higher than 0.85 (not shown). CFSR typically exhibits the best performance, followed by ERA-Interim. JRA-25 often performs better than JRA-55, perhaps because the former relies more on satellite data.

Overall, the absolute meridional moisture fluxes measured by radiosondes are lower than in the reanalyses regardless of whether the moisture is blowing north or south. The relative difference between the filtered observations and the subsampled ERA-Interim is 10.2% when averaged over all radiosonde sites (Table 2). This difference is minimal in NCEP–NCAR R1 (6.3%) and maximal in MERRA (13.2%). We sought an explanation in the representation of the humidity and wind in either dataset (Figs. 4b and 4c, respectively). Precipitable water is higher in the observations than in the reanalyses, but the meridional wind at 850 hPa (where moisture fluxes are strongest) is neither systematically higher nor lower. The mean precipitable water and wind at 850 hPa are not related to the mean vertically integrated moisture flux; this suggests that

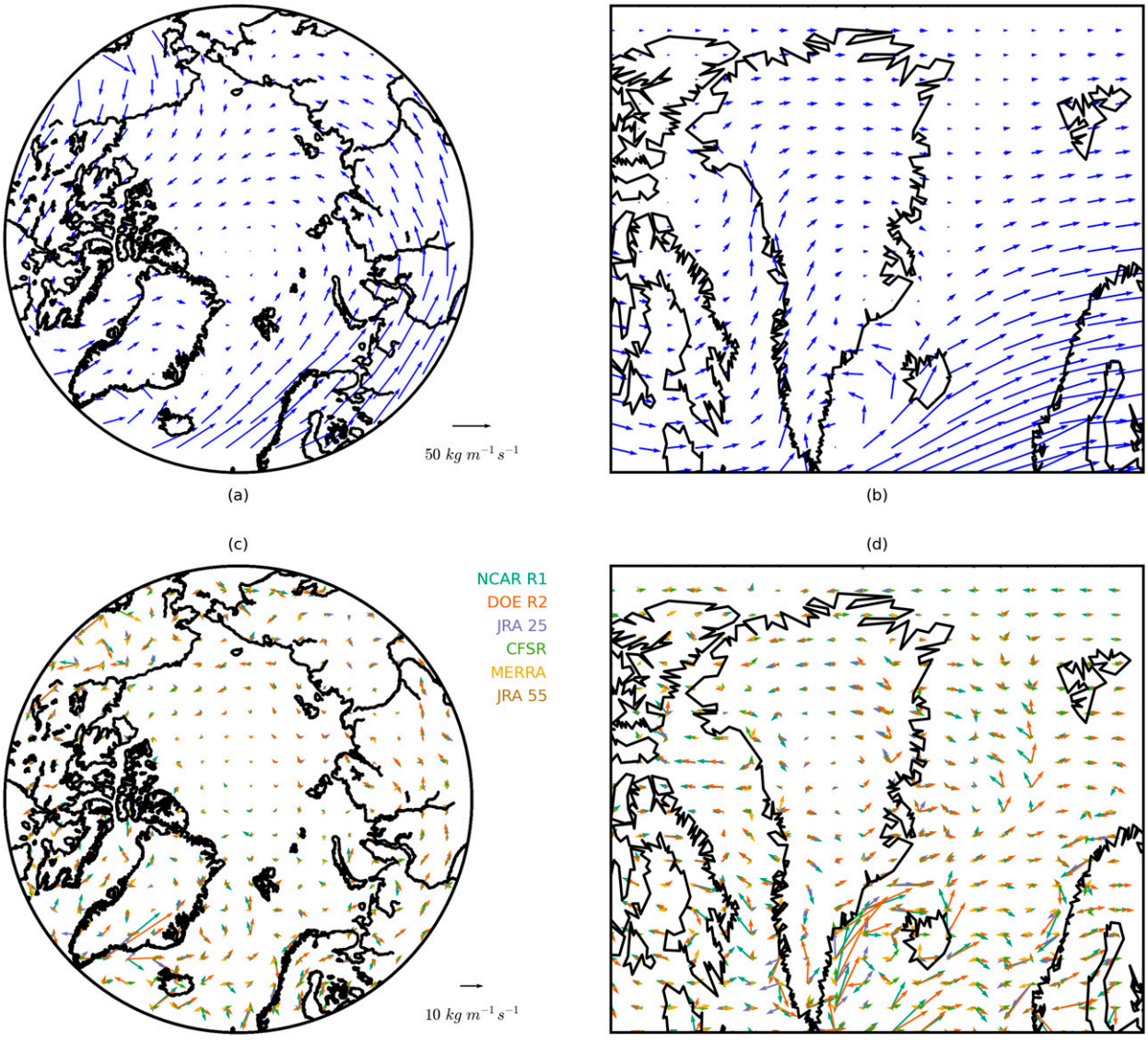

FIG. 2. Time-averaged (1979–2013) vertically integrated moisture flux north of 60°N in (a) ERA-Interim with the arrow scale (50 kg m^{-1} s^{-1}) shown at lower right of (a); and (b) a zoom on the northern North Atlantic. (c),(d) As in (a),(b), but for the differences in vertically integrated moisture flux between the other six reanalyses (different colored arrows) and ERA-Interim [arrow scale shown at lower right of (c), 10 kg m^{-1} s^{-1}].

humidity and wind are correlated, both in time and along the vertical.

The vertical profiles confirm that fluxes are weaker when derived from radiosondes and that this difference is not a side effect of the vertical integrations (Fig. 5a). The reanalyses correspond well with the observations above 700 hPa but overestimate the fluxes below that level. Only ERA-Interim and JRA-25 capture the altitude of the maximum flux, at 850 hPa. The older NCEP reanalyses place it lower, below 900 hPa, whereas CFSR, JRA-55, and MERRA have local maxima at both heights. The specific humidity is well reproduced by the reanalyses, except in the boundary layer (Fig. 5b). Below 900 hPa, the radiosonde observations report two humidity inversions not captured by the reanalyses. MERRA and JRA-55 show a single humidity inversion but overestimate its strength. The spread between datasets is greater for the mean meridional wind variable (Fig. 5c). The observed winds are weaker in the upper troposphere but are within the reanalysis envelope below 600 hPa. Below this level, the winds shift from northward to southward. This change of sign in the wind direction is absent in the moisture flux profile, indicating that the mean flow is not the main cause of moisture advection in the Arctic.

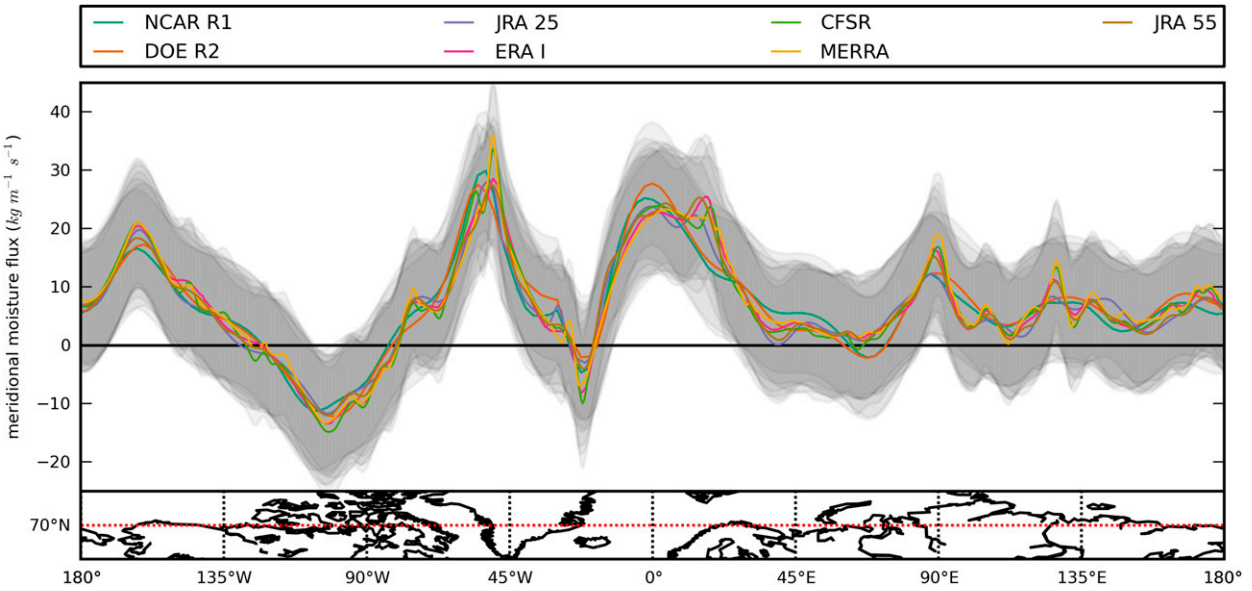

FIG. 3. Longitudinal distribution of the climatological vertically integrated meridional moisture flux at 70°N in different reanalyses (1979–2013). The gray shaded bands indicate the ranges corresponding to plus or minus one interannual standard deviation from the mean.

The vertical pattern of correlation of reanalyses' moisture transport with the IGRA is more disconcerting (Fig. 5d). ERA-Interim and CFSR systematically outmatch each other with correlation values of approximately 0.9 for the bulk of the free troposphere. These reanalyses do not perform as well near the surface or the tropopause, but this is insignificant compared with the other reanalyses, which achieve coefficients superior to

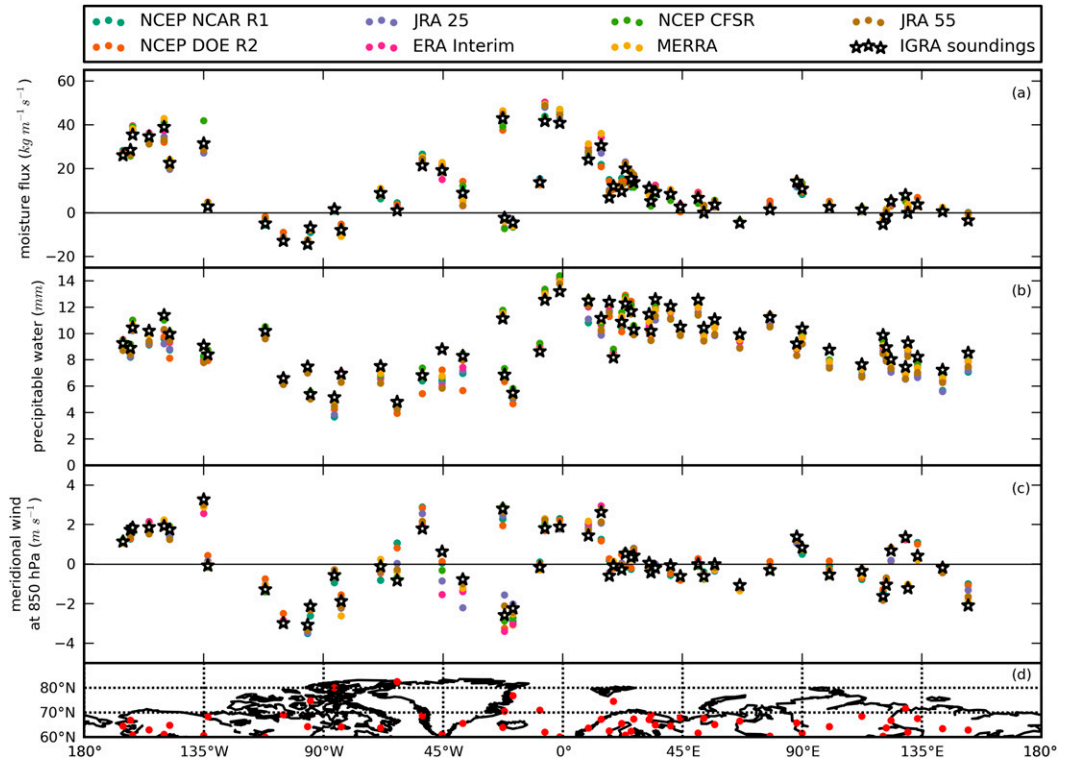

FIG. 4. (a) Climatological vertically integrated meridional moisture flux ($kg\,m^{-1}\,s^{-1}$) derived from reanalyses and radiosoundings (1979–2013) at the location of the radiosonde stations. (b),(c) As in (a), but for precipitable water (mm) and the meridional wind at 850 hPa ($m\,s^{-1}$), respectively. (d) Locations of the radiosonde stations.

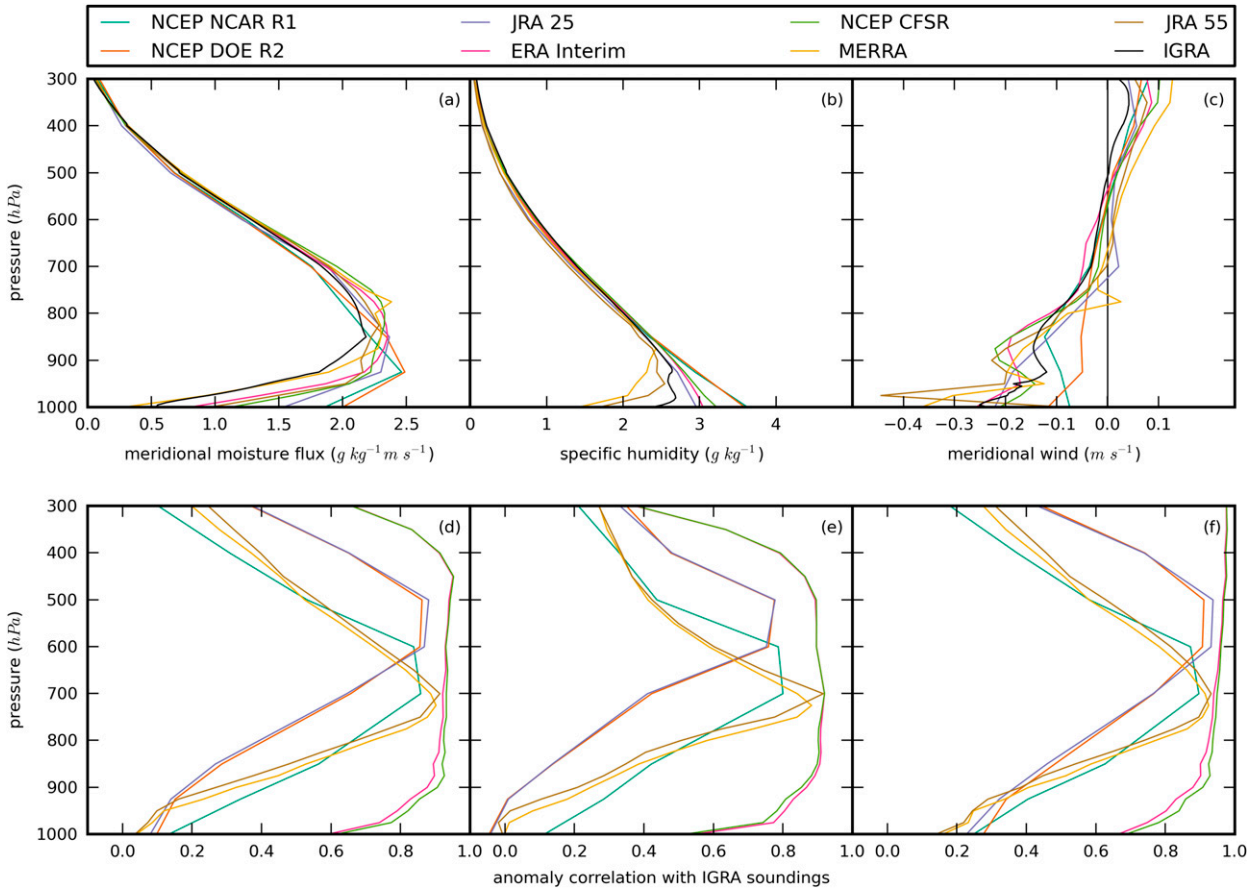

FIG. 5. Mean vertical profiles of the seven reanalyses (different colors) collocated with the selected radiosonde sites and averaged over all these sites for (a) meridional moisture flux, (b) specific humidity, and (c) meridional wind. (d)–(f) Correlations between these variables in the reanalyses and in radiosoundings.

0.8 only in the layer between 700 and 500 hPa. This result is perplexing given the high correlation with the IGRA soundings of the vertically integrated quantities in all datasets. Some datasets probably reject the radiosonde observations in the lower and upper troposphere, but the data from the midtroposphere are sufficient to reconstruct a plausible albeit inaccurate vertical profile.

The specific humidity and wind variables exhibit the same vertical correlation patterns as the moisture flux except in the upper troposphere; the wind in ERA-Interim and CFSR remains highly correlated with the soundings even higher than 500 hPa (Figs. 5e,f).

b. *Long-term moisture budgets*

Table 4 presents the terms of the moisture budget in the different datasets for four regions: north of 70°N, north of 60°N, the Arctic Ocean, and the Greenland ice sheet. The mean moisture convergence through 70°N is remarkably consistent between the seven reanalyses studied because they are constrained by common observations despite different model settings and resolutions. The minimum value (187 mm yr^{-1}) is given by JRA-25 and the maximum (203 mm yr^{-1}) by MERRA. In line with our findings in the previous subsection, the fluxes derived from radiosondes (Serreze et al. 1995) or computed from satellite data (Groves and Francis 2002) tend to be lower than the reanalysis values. Estimates of precipitation and evaporation are more scattered among datasets; net precipitation computed from model physics ranges from 95 mm yr^{-1} (NCEP–DOE R2) to 244 mm yr^{-1} (NCEP CFSR). The interdataset standard deviation for net precipitation is 45 mm yr^{-1} compared to 5.1 mm yr^{-1} for transport.

Predictably, no reanalysis succeeds in closing the moisture budget, with the largest mismatch found in NCEP–DOE R2, where the moisture convergence exceeds net precipitation by 52%. This mismatch is smaller in the other datasets (although still 34% for MERRA). CFSR exhibits the most intense water cycle. Net precipitation is higher than the moisture convergence only in CFSR and JRA-55.

For the polar cap north of 60°N, the results of Bengtsson et al. (2004a) using ERA-Interim from 1989

TABLE 4. Long-term averaged (1979–2013) moisture budget terms (mm yr^{-1}) for the polar caps north of 70°N and north of 60°N, the Arctic Ocean, and the Greenland ice sheet: T refers to the total poleward moisture transport, P to precipitation, and E to evaporation. Values in parentheses are the interannual standard deviations. This table is adapted from Cullather and Bosilovich (2011).

Region	Source	Period	P	E	$P - E$	T	$P - E - T$
70°–90°N	Serreze et al. (1995)	1974–91				163	
	Bromwich et al. (2000)	1979–93				189 (23)	
	Groves and Francis (2002)	1979–98				151	
	Jakobson and Vihma (2010)	1979–2001	323 (23)	144 (9)	179 (20)	192 (16)	−13
	Cullather and Bosilovich (2011)	1979–2005	299 (16)	167 (7)	132 (16)	205 (15)	−73
	NCEP–NCAR R1	1979–2013	295 (16)	160 (14)	135 (14)	192 (14)	−57 (12)
	NCEP–DOE R2	1979–2013	234 (21)	139 (15)	95 (15)	199 (14)	−104 (12)
	JRA-25	1979–2013	305 (17)	144 (10)	161 (19)	187 (14)	−26 (16)
	ERA-Interim	1979–2013	310 (14)	135 (9)	175 (14)	195 (13)	−20 (8)
	NCEP CFSR	1979–2013	426 (18)	181 (9)	244 (16)	192 (15)	53 (9)
	MERRA	1979–2013	300 (15)	166 (7)	134 (16)	203 (15)	−68 (16)
	JRA-55	1979–2013	350 (14)	150 (9)	200 (14)	190 (14)	10 (5)
60°–90°N	Bengtsson and al. (2011)	1989–2009	509	236	273	258	15
	NCEP–NCAR R1	1979–2013	477 (18)	300 (11)	176 (17)	270 (10)	−94 (13)
	NCEP–DOE R2	1979–2013	440 (29)	311 (18)	129 (16)	271 (11)	−142 (13)
	JRA-25	1979–2013	441 (19)	242 (7)	198 (20)	259 (9)	−61 (16)
	ERA-Interim	1979–2013	470 (13)	231 (6)	239 (13)	257 (10)	−18 (7)
	NCEP CFSR	1979–2013	623 (20)	285 (8)	338 (16)	260 (12)	78 (8)
	MERRA	1979–2013	459 (20)	280 (5)	179 (18)	266 (12)	−86 (11)
	JRA-55	1979–2013	525 (14)	258 (7)	267 (12)	260 (11)	6 (7)
Arctic Ocean	Serreze and al. (2006)	1979–2001	310	130	190	210 (21)	
	Cullather and Bosilovich (2011)	1979–2005	285 (17)	150 (8)	135 (17)	213 (17)	−78
	NCEP–NCAR R1	1979–2013	316 (16)	202 (15)	114 (16)	177 (17)	−63 (11)
	NCEP–DOE R2	1979–2013	255 (19)	191 (18)	64 (16)	193 (18)	−128 (12)
	JRA-25	1979–2013	331 (20)	192 (11)	139 (23)	175 (18)	−36 (17)
	ERA-Interim	1979–2013	340 (16)	176 (11)	164 (18)	184 (17)	−21 (9)
	NCEP CFSR	1979–2013	458 (20)	231 (12)	227 (19)	204 (18)	23 (18)
	MERRA	1979–2013	288 (16)	151 (8)	137 (17)	226 (17)	−89 (17)
	JRA-55	1979–2013	384 (16)	201 (11)	183 (18)	185 (18)	−2 (7)
Greenland	Ettema and al. (2009)	1958–2007	434 (23)	15	419		
	Burgess and al. (2010)	1979–2005			344 (23)		
	Cullather and Bosilovich (2011)	1979–2005	434 (46)	9 (2)	424 (47)	459 (44)	−35
	NCEP–NCAR R1	1979–2013	339 (26)	171 (20)	168 (28)	155 (26)	13 (26)
	NCEP–DOE R2	1979–2013	252 (29)	157 (14)	96 (28)	171 (28)	−75 (27)
	JRA-25	1979–2013	269 (24)	118 (10)	152 (25)	163 (22)	−12 (22)
	ERA-Interim	1979–2013	281 (24)	128 (12)	153 (23)	178 (22)	−24 (9)
	NCEP CFSR	1979–2013	381 (39)	146 (11)	235 (31)	289 (38)	−54 (50)
	MERRA	1979–2013	432 (44)	11 (3)	421 (45)	395 (39)	26 (19)
	JRA-55	1979–2013	308 (25)	128 (10)	180 (21)	155 (20)	25 (11)

to 2005 are congruent with our estimates from 1979 to 2013 for evaporation and transport but not precipitation (7% relative difference). Our precipitation estimates were computed as accumulated values by the numerical weather prediction model between the initialization and the first 12 h of forecast. Bengtsson et al. (2004a) preferred a time window shifted 18 h from the analysis to avoid the model spinup effects. At such lead times, net precipitation (physics output method) overshoots the transport estimates (aerological method).

We performed a similar budget analysis for the Arctic Ocean and Greenland ice sheet. Atmospheric moisture convergence represents an important source term in the Arctic freshwater budget impacting ocean stratification, convection, the intensity of the thermohaline circulation, and the formation of sea ice (Serreze et al. 2006). For Greenland, net precipitation along with meltwater runoff and blowing snow largely determines the surface mass balance of the ice sheet (Ettema et al. 2009; Burgess et al. 2010). Despite the warnings from Bengtsson et al. (2011), integrating fluxes on pressure levels has only a moderate impact on the results even over these complex domains (Table 3). The maximum relative error (3.8%) is found in MERRA over the Arctic Ocean. Even when applying the same time window (1979–2005), we were unable to reconcile our estimate of the moisture convergence over the Greenland ice sheet using MERRA (393 mm yr^{-1}) with that of Cullather and Bosilovich (2011) (459 mm yr^{-1}).

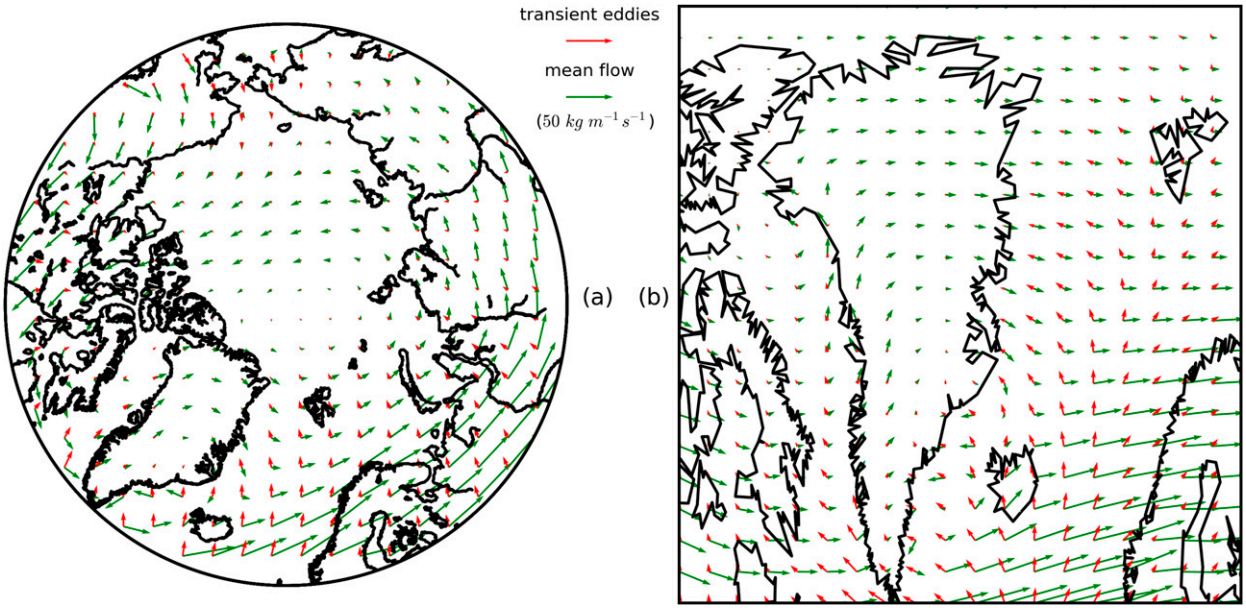

FIG. 6. Reynolds decomposition [Eq. (4)] into transient eddies (red vectors) and the men flow (green vectors) of the moisture fluxes in the ERA-Interim (a) north of 60°N and (b) a zoom over the northern North Atlantic. The same arrow scale [50 kg m^{-1} s^{-1}, shown at the top between (a) and (b)] is used for both panels.

This mismatch does not apply to precipitation and evaporation.

c. *Moisture transport due to mean flow and transient eddies*

We now turn to the analysis of the moisture transport into the Arctic using the decomposition given by Eq. (4). Figure 6 shows the climatological mean moisture transport due to the mean flow and transient eddies as represented in ERA-Interim. Driven by the westerly winds, the mean flow is largely responsible for the zonal component of the total transports. The transient eddy flux is one order of magnitude weaker but is nearly exclusively meridional, suggesting its dominant contribution to the poleward advection of moisture. However, the mean flow flux is not consistently zonal; it has relatively small meridional components. Given the large magnitude of the mean flux, it also contributes to the moisture advection toward or away from the Arctic. For example, approximately half of the total northward flux over the storm tracks is due to the mean flow component. Over the Canadian archipelago and Denmark Strait, the mean flow transport imparts a southward direction to the total transport, offsetting the effect of the transients. The explanation is found in Peixoto and Oort (1992) along with the standing wave pattern the authors identified in the mean tropopause winds. One of the two troughs is located east of the American continent, implying southward winds over Canada and northward winds over the Baffin Bay and the Greenland Sea. Over Canada, these southward winds extend to the surface, so the mean flow flux in this region is also southward. Over the Denmark Strait, the high northward winds advect a small amount of moisture compared to the southward surface winds associated with the Icelandic low because the air is more humid near the surface. As a result, the vertically integrated mean flow flux is directed south between Greenland and Iceland.

To estimate the role of the transport components in different datasets, we apply the same decomposition [Eq. (4)] to all seven reanalyses for the meridional transport component at latitude 70°N. Figure 7 illustrates that the contribution of the transient eddy transport peaks at the end of the Atlantic and Pacific storm tracks, which are common features of all reanalyses (Tilinina et al. 2013). The mean flow leads to both southward transports (e.g., at longitudes 135°–90°W, 45°–90°E) and northward transports (e.g., at 180°–135°W, 0°–45°E) that cancel each other in zonal mean. Consequently, poleward transient eddy fluxes are responsible for the bulk of the meridional moisture transport, reflecting the prominent role of cyclones in the moisture advection. The dominant role of transient eddies in the total northward moisture flux is particularly evident between 70° and 75°N for all datasets (Figs. 8a,b).

All reanalyses reveal the signature of the polar cell in the form of a southward flux of water vapor between 60° and 75°N (Fig. 8a). The vertical profile of

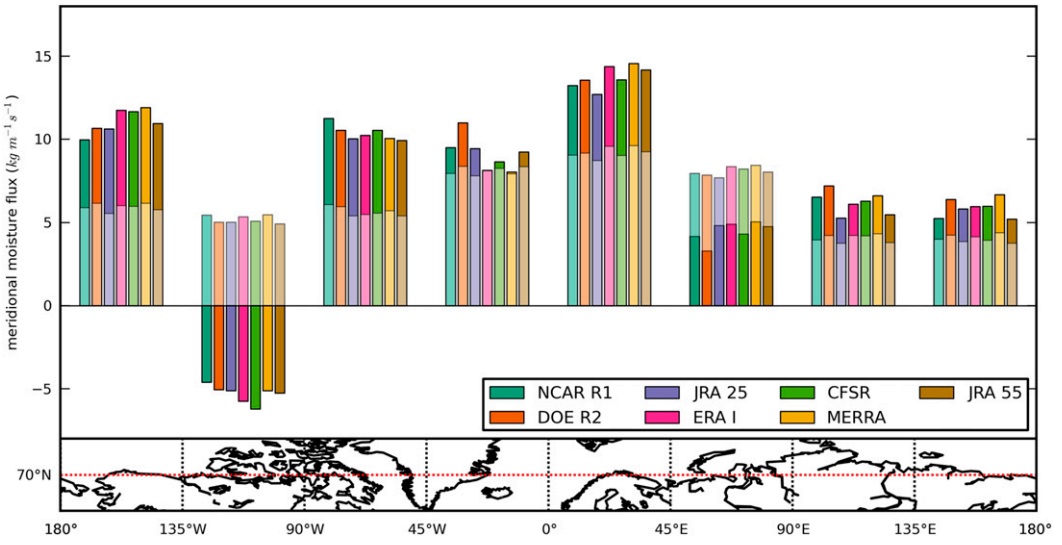

FIG. 7. Longitudinal distribution of the vertically integrated total meridional moisture transport at 70°N (dark colored portions of bars) and its transient eddy component [from Eq. (4), light colored portions] in the seven reanalyses (different colors). Each set of bars corresponds to the average over the 45°E–W longitudinal bands defined on the map in the lower panel.

the transports confirms the presence of a vertical circulation cell whose lower branch (below 600 hPa) works to advect the moist surface air toward the south (Fig. 8c). While representing only a small fraction of the total flux, this component is likely to increase (in its absolute value) in a warmer and thus moister atmosphere.

Table 5 presents the mean and standard deviation of all components of the decomposition from Eq. (5) for the moisture flux at 70°N. The residual term $\{[\overline{q}]\}\{[\overline{v}]\}$ is the mean precipitable water times the mean meridional mass flux and ranges between −4.7 (NCEP–NCAR R1) and 2.8 mm yr^{-1} (NCEP CFSR) and, in absolute value, between 0.6% (NCEP–DOE R2) and 2.4% (NCEP–NCAR R1)

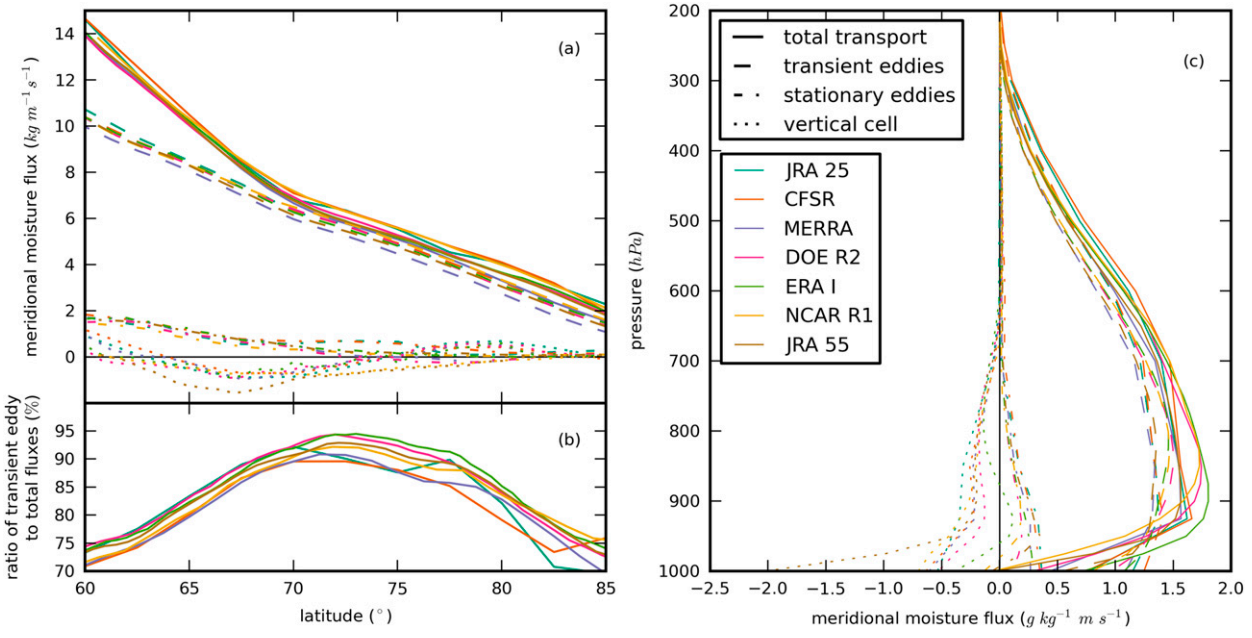

FIG. 8. Meridional distribution of (a) the absolute and (b) relative values of the different terms of the Reynolds decomposition [Eq. (5), four different types of lines] of the meridional moisture fluxes and (c) their vertical profiles at 70°N in the seven reanalyses (different colors).

TABLE 5. Long-term averaged (1979–2013) components of the moisture convergence north of 70°N (mm yr^{-1}) according to Eq. (5). Values in parentheses are the interannual standard deviations.

Reanalysis	Total $\{[\overline{qv}]\}$	Transient eddies $\{[\overline{q'v'}]\}$	Stationary eddies $\{[\overline{q}^*\overline{v}^*]\}$	Vertical cell $\{[\overline{q}]^\circ[\overline{v}]^\circ\}$	Residual $\{[\overline{q}]\}\{[\overline{v}]\}$
NCEP–NCAR R1	192 (14)	176 (10)	40 (9)	−20 (5)	−4.7 (2.4)
NCEP–DOE R2	199 (14)	178 (10)	45 (10)	−25 (7)	1.2 (2.2)
JRA-25	187 (14)	167 (9)	40 (9)	−22 (7)	2.3 (0.8)
ERA-Interim	195 (13)	180 (11)	40 (9)	−23 (6)	−1.5 (0.9)
NCEP CFSR	192 (15)	181 (11)	42 (10)	−15 (7)	2.8 (2.6)
MERRA	203 (15)	183 (11)	42 (10)	−28 (6)	−2.0 (1.1)
JRA-55	190 (14)	173 (10)	41 (10)	−23 (7)	−2.3 (0.9)

of the total convergence. The nonclosure of the mass budget of reanalyses is a known problem, particularly for NCEP–NCAR R1 (Trenberth 1997). Nevertheless, before attributing the residual term to leaking mass in the reanalyses, we note that our wind fields only extend to 200 hPa (300 hPa for NCEP–NCAR R1), which does not provide strict closure. In any case, the impact of the residual term on the moisture budget calculations is modest.

d. Seasonal variability

The seasonal variability of the moisture advection into the Arctic is important because midlatitude and subpolar storm tracks and atmospheric humidity undergo significant changes throughout the year. The seasonal march of the net precipitation over the Arctic is pronounced because precipitation and evaporation are strongly dependent on the seasonal variations in sea ice extent. All reanalyses show a similar seasonal behavior of the transport-based estimate of the moisture convergence north of 70°N (Fig. 9). The maximum of moisture convergence (~25 mm $month^{-1}$) is observed in July in all reanalyses except for NCEP–NCAR R1 and NCEP–DOE R2, which lag by one month compared to the other products. A winter minimum of about 12 mm $month^{-1}$ is observed from December to March. The moisture transport component associated with transient eddies accounts for nearly the entire moisture convergence, providing up to 90% in winter and summer and up to 100% in autumn and spring.

The annual peak of moisture transports is more acute over the radiosonde sites and occurs in September (Fig. 10a). As noted previously, the observed fluxes are weaker than in the reanalyses, particularly in spring, summer, and early autumn.

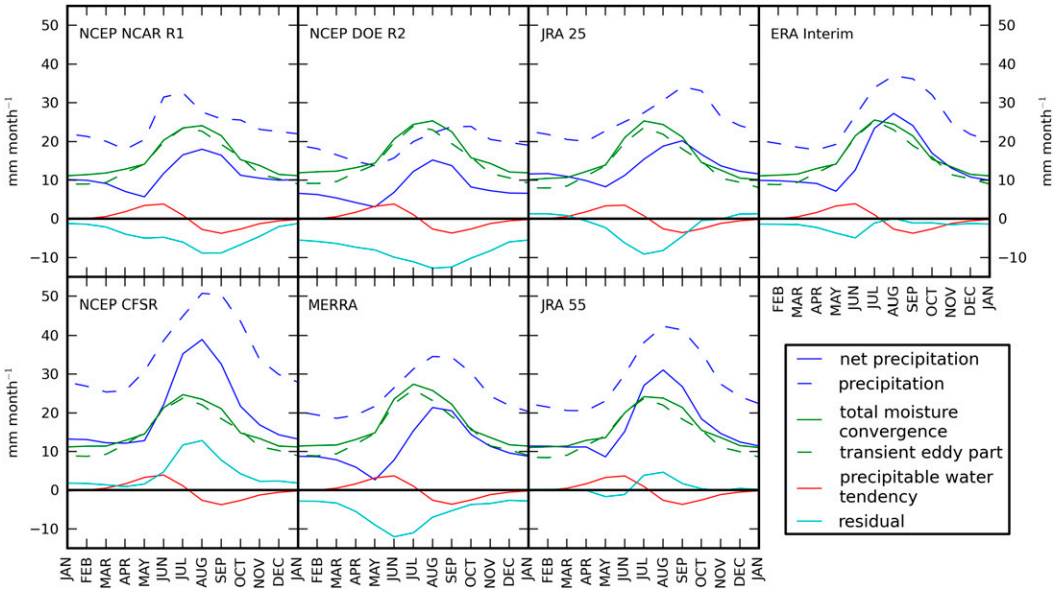

FIG. 9. Seasonal cycle of the moisture budget terms—net precipitation (solid blue), precipitation (dashed blue), total moisture convergence (solid green) and transient eddy part (dashed green), precipitable water tendency (red), and residual (cyan) for the polar cap north of 70° in the seven reanalyses. The residual term is equal to net precipitation minus convergence minus the rate of change of precipitable water.

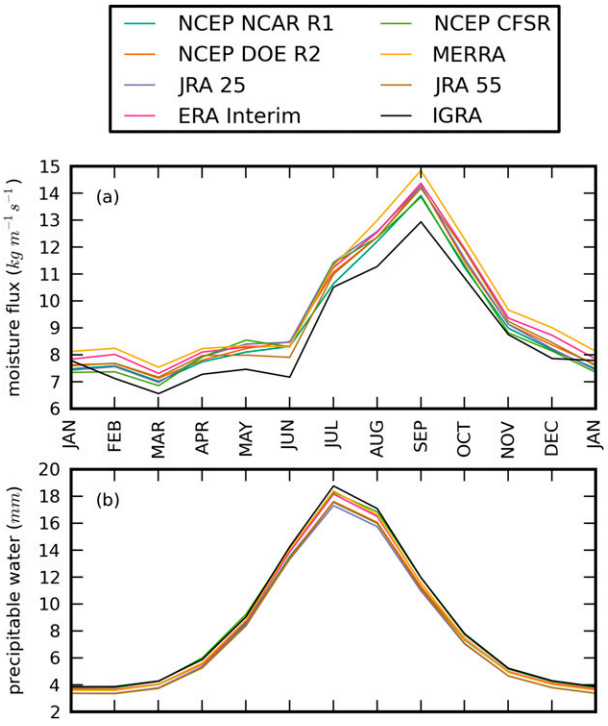

FIG. 10. Annual cycle (a) of the meridional moisture flux (kg m^{-1} s^{-1}) and (b) of precipitable water (mm) in the seven reanalyses and IGRA (different colors) averaged over all the radiosonde sites.

The maximum net precipitation lags by approximately one month with respect to the moisture convergence and is observed in August in all products, except for JRA-25, for which the maximum is observed in September. The reason for this lag is in part physical; during the warm season, the water-holding capacity of an atmospheric column increases (Fig. 9, red curve), limiting the potential for the imported and evaporated moisture to precipitate.

Figure 10b shows the annual cycle of precipitable water over the chosen radiosonde locations, which reaches a maximum in July, two months before the peak in moisture transport.

However, a portion of the lag in Fig. 9 can be interpreted as an artifact because the right- and left-hand sides of the moisture balance equation [Eq. (1)] are computed independently. The water budget is thus unlikely to be closed, as indicated by the residual term in Fig. 9 (light blue curve). The same applies to the energy budget; for example, in MERRA the surface receives an excess of 11 W m^{-2}, which could lead to excessive latent heat fluxes (Cullather and Bosilovich 2011). Indeed, in MERRA and most datasets, the closure problem is most acute in late spring, when evaporation is the highest. In contrast, the reanalyses diagnosing the most precipitation (NCEP CFSR and JRA-55) err in the opposite direction in the wet period of August and September.

We further divided the transports into the two so-called Arctic seasons: January–February–March–April (JFMA) and July–August–September–October (JASO) suggested by Tilinina et al. (2014) based on sea ice concentrations. Figure 11 shows the longitudinal distribution of total moisture fluxes as well as the transient eddy part. The local maxima are well collocated in both seasons in the subpolar North Atlantic, the Labrador Sea, and the Chukchi Sea. In these regions, the total summer fluxes are 2 to 3 times stronger compared to those in winter. This result also holds for the southward mean flow moisture flux over the Canadian Archipelago. The transient eddy fluxes in summer are also higher than in winter nearly everywhere, except for the Greenland Sea, where they are comparable. This likely results from the higher moisture in summer and the intensified storm activity over northern Eurasia and the eastern Arctic. Serreze et al. (2009) and Tilinina et al. (2013) demonstrated an intensification of cyclone activity over northern Eurasia and Canada in summer that increases the advection of moistened air, leading to a doubling of the moisture transports over these regions.

e. *Interannual variability*

We also analyzed how consistently the reanalyses reproduce the interannual variability of the Arctic moisture budget. The spread between reanalyses for the moisture transports is smaller than the interannual variability (Fig. 12a). As a result, the transport-based estimates of moisture convergence present common interannual variability patterns, such as a decade-long decline starting in 1989. During this period, the total transports decreased statistically significantly by 12% (ERA) to 15% (JRA-25). We computed linear trends with different time windows to evaluate how robust these patterns were. Unlike MERRA (Fig. 12b), the significance of the trends in ERA-Interim (Fig. 12c) is very sensitive to the starting year of the record; 1989 was a year of exceptionally strong fluxes. The impact of 1989 is evident in all reanalyses with the exception of MERRA. Over the 1979–2013 period, the trends in moisture transport are not statistically different from zero.

The Reynolds decomposition of the moisture flux gives some insight into the post-1989 decline. During this period, the transient eddy fluxes remained constant (Fig. 13a), but the contribution of stationary eddies and the polar cell dropped (Figs. 13b,c). The transport by the mean flow was responsible for the weakening of the meridional total moisture flux; by the turn of the millennium, transient eddies provided the totality of the moisture flux (Fig. 13d).

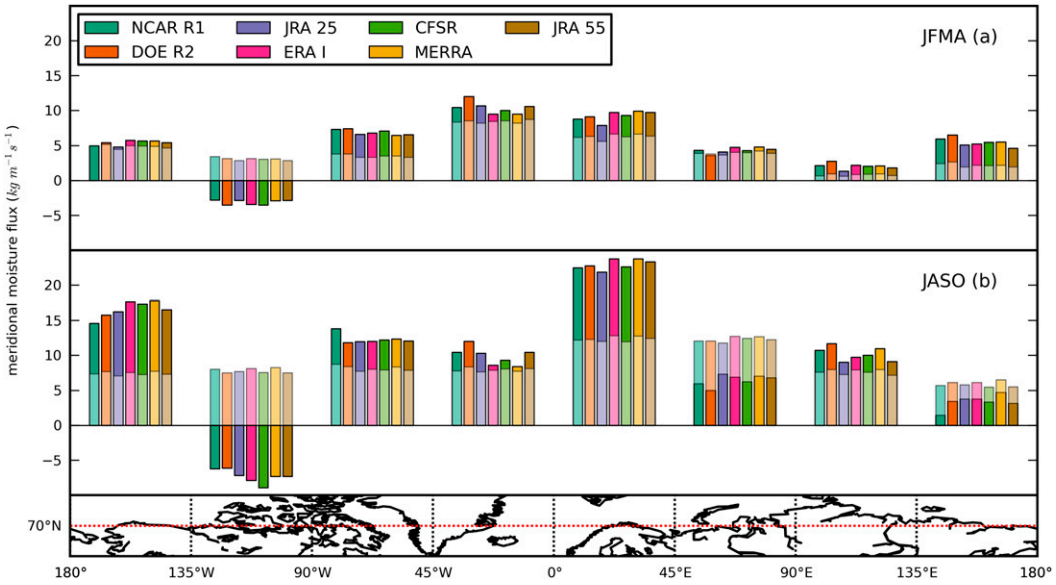

FIG. 11. As in Fig. 7, but for (a) the Arctic winter season (JFMA) and (b) the Arctic summer season (JASO).

The time series of the moisture budget components confirm the disparity in evaporation and precipitation estimates as opposed to the transport products (Figs. 13e,f,g). Precipitation and evaporation are on the rise with the strongest signals identified in NCEP–DOE R2 for evaporation (9.7% decade^{-1}) and in JRA-55 for evaporation also (4.6% decade^{-1}). The reanalyses disagree as to the sign of the net precipitation change. Unlike the two JRAs, most report an increase, with statistical significance in MERRA.

The nonclosure of the moisture budget is accounted for in the residual term. The 1990s and the early 2000s has seen a reduction in the absolute value of the residual in several datasets, most conspicuously in NCEP–NCAR R1, JRA-25, ERA-Interim, and MERRA. In the former, the sharp decrease (in absolute value) between 1998 and 1999 can be related to the introduction of the Advanced Microwave Sounding Unit (AMSU) in November 1998, as suggested by Cullather and Bosilovich (2011).

Figures 13i,j show the comparison between reanalyses and IGRA data for meridional moisture fluxes and precipitable water, respectively. The radiosoundings indicate weaker moisture transport in the 1980s than the reanalyses, but after 1989, the different transport estimates are highly consistent. Changes in precipitable water content are also very consistent across datasets, showing upward trends ranging from 5.0% to 9.8% over the 35-yr period, with statistical significance at the 95% level. A joint consideration of changes in the total meridional moisture transport and precipitable water reveals an apparent paradox. On the one hand, neither observations nor reanalyses report any significant change in northward moisture fluxes (Fig. 13i). On the other hand, precipitable water has increased unambiguously in all datasets (Fig. 13j). The increases in specific humidity have therefore not translated into corresponding increases in moisture fluxes. This goes against the widespread argument that the poleward moisture fluxes should strengthen in a warmer climate; it vindicates the opposing thesis, that the intensification of the hydrological cycle is driven locally by evaporation (Bintanja and Selten 2014).

Given that moisture fluxes depend on both humidity and wind, a reasonable question arises: Could changes in winds compensate the moistening? To solve this conundrum, we introduce a more compact decomposition of the mean moisture fluxes through 70°N:

$$\{[\overline{qv}]\} = \{[\overline{q'^{*\circ}v'^{*\circ}}]\} + \{[\overline{q}]\}\{[\overline{v}]\}, \tag{6}$$

where $q'^{*\circ} = q - \{[\overline{q}]\}$ and $v'^{*\circ} = v - \{[\overline{v}]\}$ (i.e., anomalies relative to the vertical, zonal, and monthly mean). The first term on the right-hand side of Eq. (6) is the covariance between the specific humidity and meridional wind. The second term is small, as shown in Table 5, and we ignore it. We represent the covariance as the product of the standard deviation of the humidity and wind and their mutual correlation:

$$\{[\overline{qv}]\} = \sigma_{t,\lambda,p} q\, \sigma_{t,\lambda,p} v\ \mathrm{corr}_{t,\lambda,p}(q, v). \tag{7}$$

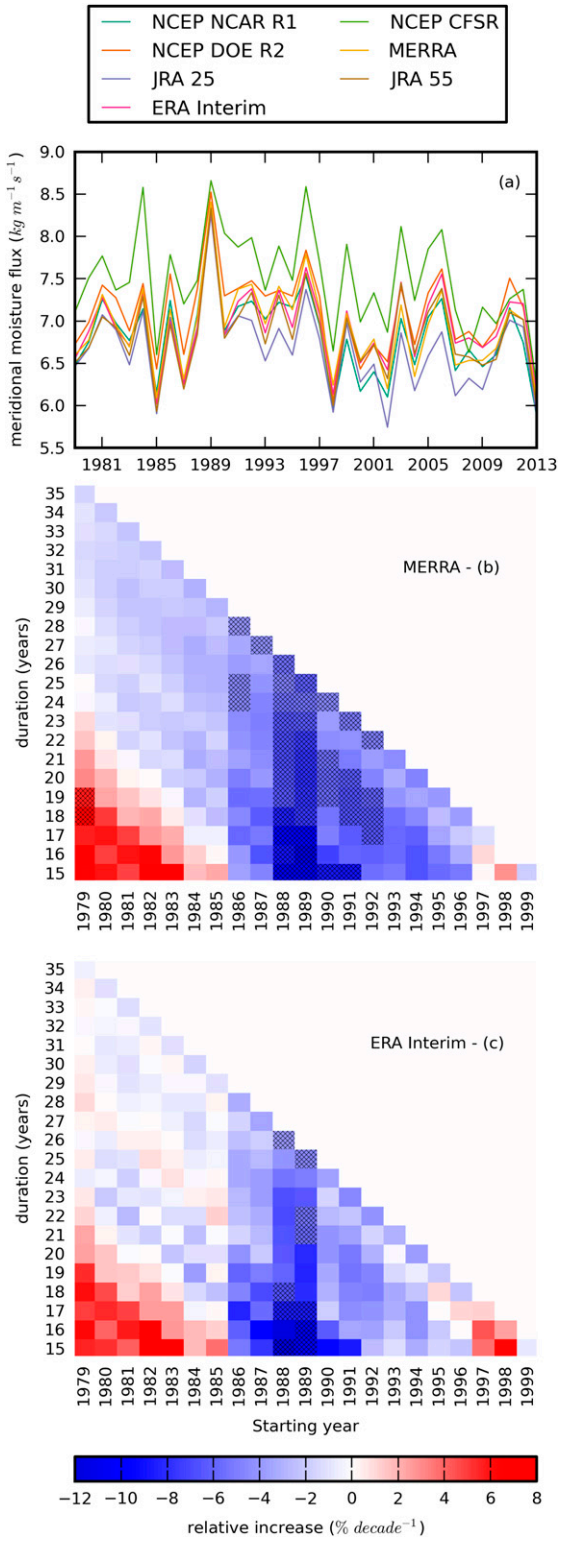

FIG. 12. (a) The time series of the mean meridional moisture flux ($kg\,m^{-1}\,s^{-1}$) through 70°N in all seven reanalyses (different colors). Slope of the linear trend of this flux for (b) MERRA and (c) ERA-Interim for different years from 1979 to 1999. Blocks with hatching are statistically significant.

The evolution of the three factors over time is plotted in Fig. 14.

The standard deviation of the humidity increased in all datasets from 7.5% (JRA-25) to 12.9% (MERRA), with statistical significance in NCEP–NCAR R1, JRA-25, ERA-Interim, and JRA-55 (Fig. 14a). The variance in humidity can be written as the sum of the temporal variance, the zonal variance, and the vertical variance in much the same manner as the moisture flux in Eq. (5):

$$\sigma^2_{t,\lambda,p}q = \{[\sigma^2_t q]\} + [\sigma^2_\lambda \overline{q}] + \sigma^2_p[\overline{q}]. \tag{8}$$

The first term on the left-hand side, the temporal variability, only contributes slightly to the increase in the total variance (6%–16%, depending on the reanalysis). The second and third terms represent the spatial variability, in both longitude and height. The saturation specific humidity depends exponentially on temperature through the Clausius–Clapeyron relation. If the atmosphere warms homogeneously and the relative humidity remains constant, the humid regions moisten faster than the dry regions. For example, the humidity contrast between the surface and the higher troposphere becomes sharper; $\sigma^2_p[\overline{q}]$ comprises 83%–89% of the increase in the total variance. The contribution of the zonal variance is considerably smaller (−3% to 7%).

The standard deviation of the meridional wind remained approximately constant with a slight decrease in some reanalyses that was never statistically significant (Fig. 14b). The correlation between wind and humidity decreased significantly in all datasets but one (NCEP–DOE R2), as shown in Fig. 14c, which led to the slight decrease in the moisture flux (Fig. 14d) in spite of the moistening. The increasing humidity did not result in stronger moisture fluxes because the moisture and wind variations in space and time do not correspond as well as in previous periods.

Figure 15a shows that the moisture flux has decreased below 700 hPa and increased moderately above. To explain this, we consider the correlation between the meridional wind speed and humidity to determine which levels have contributed most to the $\mathrm{corr}_{t,\lambda,p}(q, v)$ statistic. We introduce a normalized flux: $[\overline{qv}]/(\sigma_{t,\lambda,p}q\,\sigma_{t,\lambda,p}v)$; its vertical integral is exactly $\mathrm{corr}_{t,\lambda,p}(q, v)$ according to Eq. (8). The normalized flux has decreased particularly near the surface, between 950 and 850 hPa depending on the reanalysis (Fig. 15b). At these altitudes, the prevailing wind blows south, as part of the lower branch of the polar cell. However, this is only part of the explanation because the moisture transports due to the polar cell have not changed significantly (Fig. 13c).

The link between increases in moisture and transports is therefore not straightforward. The analysis of trends is

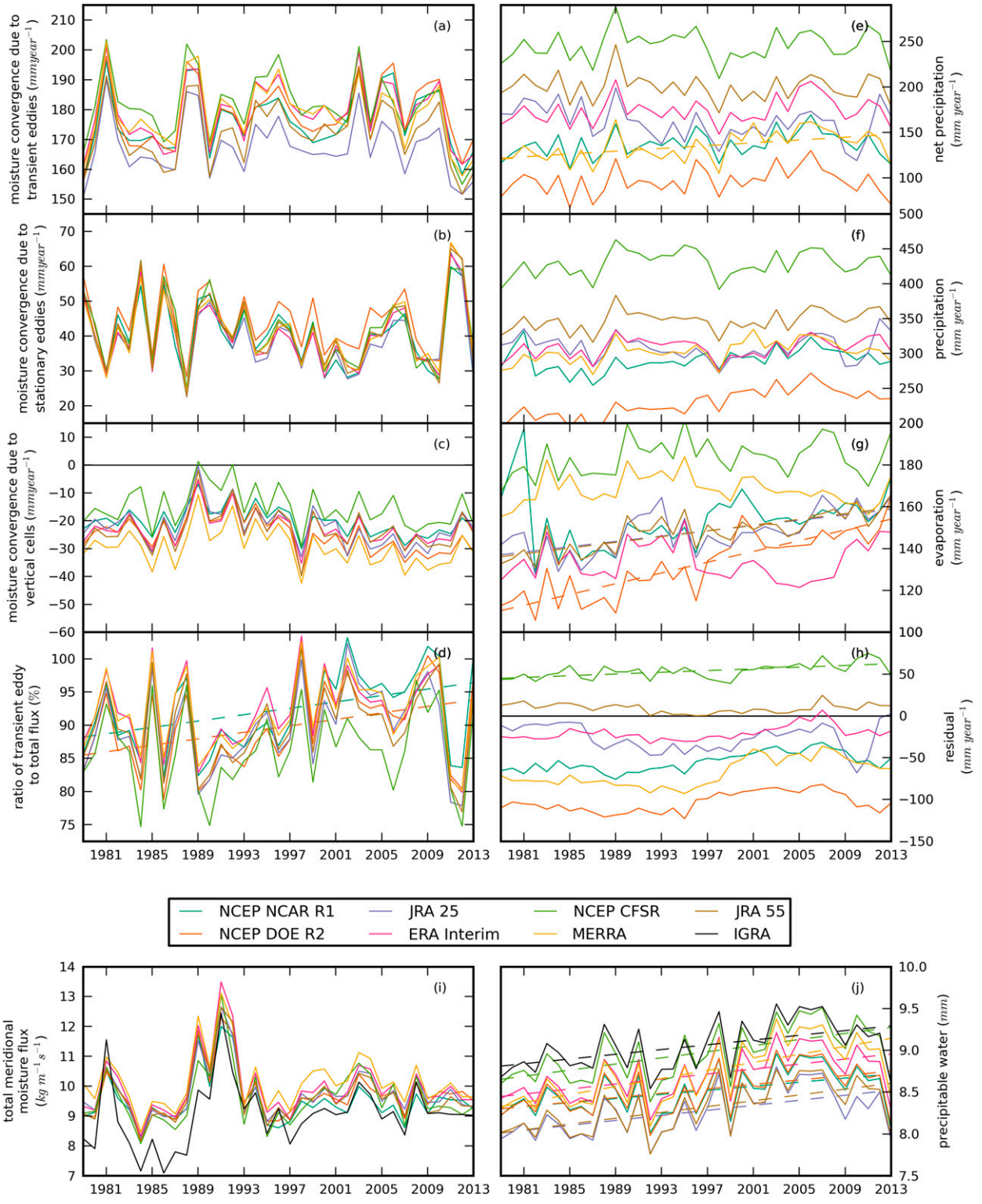

FIG. 13. Time series (1981–2013) of moisture convergence (mm yr^{-1}) in the polar cap north of 70°N via the aerological method decomposed into (a) the transient eddy part, (b) the stationary eddy part, and (c) the vertical cell according to Eq. (5) for the seven reanalyses and IGRA (different colors). (d) The transient eddy part divided by the total flux. Time series of the terms of the moisture budget (mm yr^{-1}) for this region for the seven reanalyses: (e) net precipitation, or $P - E$, via the physics output method, (f) precipitation, (g) evaporation, and (h) the residual (i.e., the difference between the physics output and the aerological methods). (i) The meridional moisture flux (kg m^{-1} s^{-1}) in the reanalyses and IGRA averaged over all selected stations; (j) as in (i), but for the precipitable water variable (mm). The regression line of a given variable is drawn (in dashes) if its trend is statistically significant at the 95% level (Student's t test).

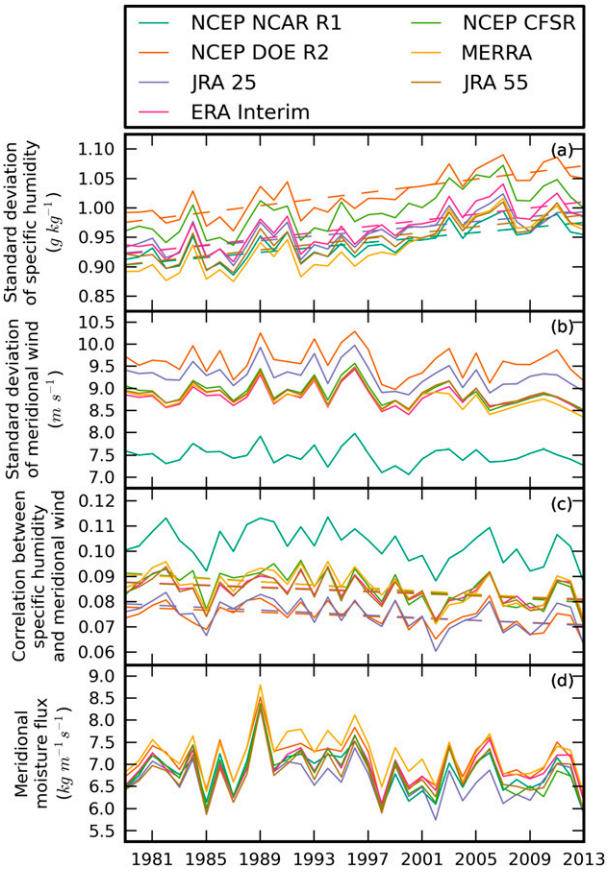

FIG. 14. The covariance of meridional wind and specific humidity at 70°N vs year (1979–2013) for the seven reanalyses (different colors) decomposed into (a) the standard deviation of specific humidity ($g\,kg^{-1}$), (b) the standard deviation of meridional wind ($m\,s^{-1}$), and (c) the correlation between both variables according to Eq. (7). (d) For the same years, the vertically integrated moisture flux ($kg\,m^{-1}\,s^{-1}$) through 70°N. Regression lines are drawn (in dashes) if the trends are statistically significant.

impeded by strong interannual variability dominating the long-term tendencies. At the same time, climate models consistently project an increase in the moisture fluxes to the Arctic for the twenty-first century (e.g., Hwang et al. 2011). The departure from the simple Clausius–Clapeyron scaling of the moisture fluxes could be a transitory phenomenon that would lapse when the global warming signal becomes stronger.

5. Conclusions and discussion

We analyzed the Arctic moisture budget in seven reanalyses for the 1979–2013 period. The evaluation of the atmospheric moisture transport in the reanalyses against the radiosonde data demonstrated a qualitative agreement in terms of longitudinal, vertical, and temporal patterns but also a quantitative difference—that

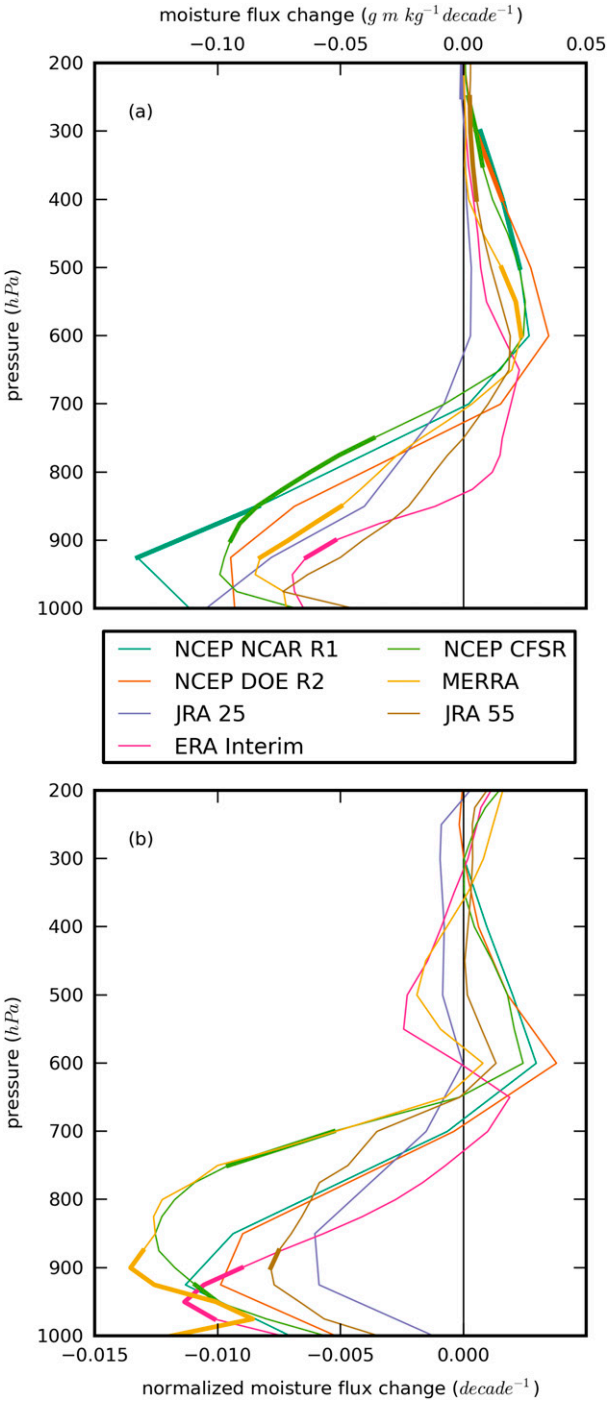

FIG. 15. (a) Vertical profile of the trend in meridional moisture flux ($g\,m\,kg^{-1}\,s^{-1}\,decade^{-1}$) at 70°N for the seven reanalyses (different colors). Bold portions of lines correspond to statistically significant trends. (b) Vertical profile of the trend in normalized moisture flux ($decade^{-1}$). The normalized flux is defined as $[\overline{qv}]/(\sigma_{t,\lambda,p}q\,\sigma_{t,\lambda,p}v)$.

is, a 6%–13% overestimation of the moisture fluxes by the reanalyses compared to in situ data. The variation in the estimates of the net precipitation in different products over the Arctic is large compared to the moisture flux. Although both variables have similar mean values, the set-to-set standard deviation of the net precipitation is nearly 10 times that of the moisture convergence (45 vs 5.1 mm yr^{-1}). Meridional moisture transport in the Arctic is largely dominated by transient eddies, which explain 88%–94% of the total moisture transports at 70°N. The reason for this result is the averaging of the mean flow fluxes; the regions of northward fluxes (the North Atlantic, Baffin Bay, and the North Pacific) are offset by regions of southward mean flow (over Canada and western Russia). In contrast, the transient eddy transports are always northward, with peaks along the storm tracks. In spite of the magnitude of the annual cycle, with transports almost doubling from winter to summer, differences between datasets remain minor throughout the year. The interannual variability, as evidenced by linear trends, is not as consistent among datasets. Most datasets depict a locally driven intensification of the water cycle; precipitation increases because of changes in local evaporation, not because of moisture imports. Growing atmospheric humidity in the lower troposphere does not result in an increase of the northward moisture transport because the correlation of humidity and meridional wind at these levels has weakened.

Although transient eddies dominate moisture advection, several studies have shown how dependent they are on larger temporal- and spatial-scale patterns. Sorteberg and Walsh (2008) demonstrated that cyclones entering the Arctic are largely responsible for the poleward moisture advection, but they also noted that the number of cyclones passing over the Greenland Sea depends on large-scale circulation patterns, as reported earlier by Tsukernik et al. (2007). Woods et al. (2013) also argued along these lines, positing that blocking high pressure systems steer cyclones toward the pole and lead to intense moisture intrusions. In this respect, further analysis should be conducted to clarify the interplay between transient eddies and the large-scale flow, relying on a detailed analysis of cyclone activity (Tilinina et al. 2013, 2014) as well as an improved Reynolds decomposition with different temporal cutoffs, as in Newman et al. (2012).

Similar studies with refined diagnostics can be extended to regional and long-term reanalyses. A natural choice would be the recent Arctic System Reanalysis (Bromwich et al. 2015), which was produced with a high-resolution version of the nonhydrostatic Polar Weather Research and Forecasting Model and assimilated more data regionally than the global reanalyses. Nevertheless, to understand the Arctic hydrological cycle on multidecadal time scales, it is important to examine reanalyses not limited to the satellite era, such as NOAA ESRL Twentieth Century Reanalysis (Compo et al. 2011), ERA-20C, and ERA CLIM (Hersbach et al. 2015). The analysis of moisture transports in these products would enable an understanding of the mechanisms steering the Arctic hydrological cycle during the time of the so-called early twentieth-century Arctic warming (Bengtsson et al. 2004b; Yamanouchi 2011). These datasets could then constitute a standard to evaluate the historical runs of the CMIP5 ensemble of climate models and to clarify the extent to which they reproduce the features of the Arctic hydrological cycle and their changes in a warming climate. Existing assessments of multimodel projections of the Arctic hydrological cycle (Kattsov and Walsh 2000; Kattsov et al. 2007; Rawlins et al. 2010) mainly cover evaporation and precipitation along with river discharge. These assessments will benefit from estimates of moisture advection, which shed more light on the mechanisms of change and the model capabilities to represent these mechanisms. Moreover, the evaluation of changes in the atmospheric moisture budget can be further related to the variations in the Arctic Ocean freshwater budget (Holland et al. 2007; Koenigk et al. 2007), providing a comprehensive assessment of all sources and sinks of freshwater in the northern high latitudes.

Acknowledgments. The critical comments and useful suggestions of the two anonymous reviewers helped to improve the paper considerably and were greatly appreciated. This work was supported by the project ''Mechanisms of moisture advection in high latitudes in the present and future climate'' funded by CNRS and UJF, the ARCTIC-ERA project funded by Agence Nationale de la Recherche (ANR) through the Belmont Fund initiative, and the GREENICE-61841 project funded by NordForsk. OZ and SKG also benefited from Grant 14.B25.31.0026 from the Russian Ministry of Education and Science. Atmospheric reanalysis data were made available courtesy of the NOAA National Centers for Environmental Prediction (NCEP), NASA, European Centre for Medium-Range Weather Forecasts (ECMWF), and Japan Meteorological Agency (JMA).

REFERENCES

Bengtsson, L., S. Hagemann, and K. I. Hodges, 2004a: Can climate trends be calculated from reanalysis data? *J. Geophys. Res.*, **109**, D11111, doi:10.1029/2004JD004536.

——, V. A. Semenov, and O. M. Johannessen, 2004b: The early twentieth-century warming in the Arctic—A possible mechanism. *J. Climate*, **17**, 4045–4057, doi:10.1175/1520-0442(2004)017<4045:TETWIT>2.0.CO;2.

——, K. I. Hodges, S. Koumoutsaris, M. Zahn, and N. Keenlyside, 2011: The changing atmospheric water cycle in polar regions in a warmer climate. *Tellus*, **63A**, 907–920, doi:10.1111/j.1600-0870.2011.00534.x.

Bintanja, R., and F. Selten, 2014: Future increases in arctic precipitation linked to local evaporation and sea-ice retreat. *Nature*, **509**, 479–482, doi:10.1038/nature13259.

Boisvert, L. N., T. Markus, and T. Vihma, 2013: Moisture flux changes and trends for the entire Arctic in 2003–2011 derived from EOS Aqua data. *J. Geophys. Res. Oceans*, **118**, 5829–5843, doi:10.1002/jgrc.20414.

Bosilovich, M., and Coauthors, 2006: NASA's Modern-Era Retrospective Analysis for Research and Applications (MERRA). *U.S. CLIVAR Variations*, No. 4, 5–8.

Bromwich, D., R. Cullather, and M. Serreze, 2000: Reanalyses' depictions of the Arctic atmospheric moisture budget. *The Freshwater Budget of the Arctic Ocean*, Springer, 163–196.

——, A. B. Wilson, L.-S. Bai, G. W. K. Moore, and P. Bauer, 2015: A comparison of the regional Arctic System Reanalysis and the global ERA-Interim reanalysis for the Arctic. *Quart. J. Roy. Meteor. Soc.*, **142**, 644–658, doi:10.1002/qj.2527.

Burgess, E. W., R. R. Forster, J. E. Box, E. Mosley-Thompson, D. H. Bromwich, R. C. Bales, and L. C. Smith, 2010: A spatially calibrated model of annual accumulation rate on the Greenland ice sheet (1958–2007). *J. Geophys. Res.*, **115**, F02004, doi:10.1029/2009JF001293.

Collins, M., and Coauthors, 2013: Long-term climate change: Projections, commitments and irreversibility. *Climate Change 2013: The Physical Science Basis*, T. F. Stocker et al., Eds., Cambridge University Press, 1029–1136. [Available online at http://www.climatechange2013.org/images/report/WG1AR5_Chapter12_FINAL.pdf.]

Compo, G. P., and Coauthors, 2011: The Twentieth Century Reanalysis Project. *Quart. J. Roy. Meteor. Soc.*, **137**, 1–28, doi:10.1002/qj.776.

Cullather, R. I., and M. G. Bosilovich, 2011: The moisture budget of the polar atmosphere in MERRA. *J. Climate*, **24**, 2861–2879, doi:10.1175/2010JCLI4090.1.

——, D. H. Bromwich, and M. C. Serreze, 2000: The atmospheric hydrologic cycle over the Arctic Basin from reanalyses. Part I: Comparison with observations and previous studies. *J. Climate*, **13**, 923–937, doi:10.1175/1520-0442(2000)013<0923:TAHCOT>2.0.CO;2.

Dee, D., and Coauthors, 2011: The ERA-Interim reanalysis: Configuration and performance of the data assimilation system. *Quart. J. Roy. Meteor. Soc.*, **137**, 553–597, doi:10.1002/qj.828.

Durre, I., R. S. Vose, and D. B. Wuertz, 2006: Overview of the integrated global radiosonde archive. *J. Climate*, **19**, 53–68, doi:10.1175/JCLI3594.1.

Ebita, A., and Coauthors, 2011: The Japanese 55-year Reanalysis "JRA-55": An interim report. *SOLA*, **7**, 149–152, doi:10.2151/sola.2011-038.

Ettema, J., M. R. van den Broeke, E. van Meijgaard, W. J. van de Berg, J. L. Bamber, J. E. Box, and R. C. Bales, 2009: Higher surface mass balance of the Greenland ice sheet revealed by high-resolution climate modeling. *Geophys. Res. Lett.*, **36**, L12501, doi:10.1029/2009GL038110.

Francis, J. A., 2002: Validation of reanalysis upper-level winds in the Arctic with independent rawinsonde data. *Geophys. Res. Lett.*, **29**, 1315, doi:10.1029/2001GL014578.

Grant, A., S. Brönnimann, and L. Haimberger, 2008: Recent arctic warming vertical structure contested. *Nature*, **455**, E2–E3, doi:10.1038/nature07257.

Groves, D. G., and J. A. Francis, 2002: Moisture budget of the arctic atmosphere from TOVS satellite data. *J. Geophys. Res.*, **107**, 4391, doi:10.1029/2001JD001191.

Hartmann, D., and Coauthors, 2013: Observations: Atmosphere and surface. *Climate Change 2013: The Physical Science Basis*, T. F. Stocker et al., Eds., Cambridge University Press, 159–254.

Hersbach, H., C. Peubey, A. Simmons, P. Berrisford, P. Poli, and D. Dee, 2015: ERA-20CM: A twentieth-century atmospheric model ensemble. *Quart. J. Roy. Meteor. Soc.*, **141**, 2350–2375, doi:10.1002/qj.2528.

Holland, M. M., J. Finnis, A. P. Barrett, and M. C. Serreze, 2007: Projected changes in Arctic Ocean freshwater budgets. *J. Geophys. Res.*, **112**, G04S55, doi:10.1029/2006JG000354.

Hwang, Y.-T., D. M. Frierson, and J. E. Kay, 2011: Coupling between arctic feedbacks and changes in poleward energy transport. *Geophys. Res. Lett.*, **38**, L17704, doi:10.1029/2011GL048546.

Jakobson, E., and T. Vihma, 2010: Atmospheric moisture budget in the Arctic based on the ERA-40 reanalysis. *Int. J. Climatol.*, **30**, 2175–2194, doi:10.1002/joc.2039.

Kalnay, E., and Coauthors, 1996: The NCEP/NCAR 40-Year Reanalysis Project. *Bull. Amer. Meteor. Soc.*, **77**, 437–471, doi:10.1175/1520-0477(1996)077<0437:TNYRP>2.0.CO;2.

Kanamitsu, M., W. Ebisuzaki, J. Woollen, S.-K. Yang, J. Hnilo, M. Fiorino, and G. Potter, 2002: NCEP–DOE AMIP-II Reanalysis (R-2). *Bull. Amer. Meteor. Soc.*, **83**, 1631–1643, doi:10.1175/BAMS-83-11-1631.

Kattsov, V. M., and J. E. Walsh, 2000: Twentieth-century trends of arctic precipitation from observational data and a climate model simulation. *J. Climate*, **13**, 1362–1370, doi:10.1175/1520-0442(2000)013<1362:TCTOAP>2.0.CO;2.

——, ——, W. L. Chapman, V. A. Govorkova, T. V. Pavlova, and X. Zhang, 2007: Simulation and projection of arctic freshwater budget components by the IPCC AR4 global climate models. *J. Hydrometeor.*, **8**, 571–589, doi:10.1175/JHM575.1.

Kobayashi, S., and Coauthors, 2015: The JRA-55 reanalysis: General specifications and basic characteristics. *J. Meteor. Soc. Japan*, **93**, 5–48.

Koenigk, T., U. Mikolajewicz, H. Haak, and J. Jungclaus, 2007: Arctic freshwater export in the 20th and 21st centuries. *J. Geophys. Res.*, **112**, G04S41, doi:10.1029/2006JG000274.

Kopec, B. G., X. Feng, F. A. Michel, and E. S. Posmentier, 2016: Influence of sea ice on arctic precipitation. *Proc. Natl. Acad. Sci. USA*, **113**, 46–51, doi:10.1073/pnas.1504633113.

Liu, C., and E. A. Barnes, 2015: Extreme moisture transport into the Arctic linked to Rossby wave breaking. *J. Geophys. Res. Atmos.*, **120**, 3774–3788, doi:10.1002/2014JD022796.

Newman, M., G. N. Kiladis, K. M. Weickmann, F. M. Ralph, and P. D. Sardeshmukh, 2012: Relative contributions of synoptic and low-frequency eddies to time-mean atmospheric moisture transport, including the role of atmospheric rivers. *J. Climate*, **25**, 7341–7361, doi:10.1175/JCLI-D-11-00665.1.

Onogi, K., and Coauthors, 2007: The JRA-25 Reanalysis. *J. Meteor. Soc. Japan*, **85**, 369–432, doi:10.2151/jmsj.85.369.

Oshima, K., and K. Yamazaki, 2006: Difference in seasonal variation of net precipitation between the arctic and Antarctic regions. *Geophys. Res. Lett.*, **33**, L18501, doi:10.1029/2006GL027389.

Peixoto, J., and A. H. Oort, 1992: *Physics of Climate*. American Institute of Physics, 520 pp.

Polyakov, I. V., and Coauthors, 2002: Observationally based assessment of polar amplification of global warming. *Geophys. Res. Lett.*, **29**, 1878, doi:10.1029/2001GL011111.

Rančić, M., J. Derber, D. Parrish, R. Treadon, and D. Kleist, 2008: The development of the first-order time extrapolation to the observation (FOTO) method and its application in the NCEP global data assimilation system. *12th Conf. on IOAS-AOLS*, New Orleans, LA, Amer. Meteor. Soc., J6.1. [Available online at https://ams.confex.com/ams/88Annual/techprogram/paper_131816.htm.]

Rawlins, M. A., and Coauthors, 2010: Analysis of the arctic system for freshwater cycle intensification: Observations and expectations. *J. Climate*, **23**, 5715–5737, doi:10.1175/2010JCLI3421.1.

Rienecker, M. M., and Coauthors, 2011: MERRA: NASA's Modern-Era Retrospective Analysis for Research and Applications. *J. Climate*, **24**, 3624–3648, doi:10.1175/JCLI-D-11-00015.1.

Saha, S., and Coauthors, 2010: The NCEP Climate Forecast System Reanalysis. *Bull. Amer. Meteor. Soc.*, **91**, 1015–1057, doi:10.1175/2010BAMS3001.1.

Screen, J. A., and I. Simmonds, 2010: The central role of diminishing sea ice in recent arctic temperature amplification. *Nature*, **464**, 1334–1337, doi:10.1038/nature09051.

Seager, R., and N. Henderson, 2013: Diagnostic computation of moisture budgets in the ERA-Interim reanalysis with reference to analysis of CMIP-archived atmospheric model data. *J. Climate*, **26**, 7876–7901, doi:10.1175/JCLI-D-13-00018.1.

Serreze, M. C., R. G. Barry, and J. E. Walsh, 1995: Atmospheric water vapor characteristics at 70°N. *J. Climate*, **8**, 719–731, doi:10.1175/1520-0442(1995)008<0719:AWVCA>2.0.CO;2.

——, and Coauthors, 2006: The large-scale freshwater cycle of the Arctic. *J. Geophys. Res.*, **111**, C11010, doi:10.1029/2005JC003424.

——, A. Barrett, J. Stroeve, D. Kindig, and M. Holland, 2009: The emergence of surface-based arctic amplification. *Cryosphere*, **3**, 11–19, doi:10.5194/tc-3-11-2009.

Sorteberg, A., and J. E. Walsh, 2008: Seasonal cyclone variability at 70°N and its impact on moisture transport into the Arctic. *Tellus*, **60A**, 570–586, doi:10.1111/j.1600-0870.2008.00314.x.

Stroeve, J. C., M. C. Serreze, M. M. Holland, J. E. Kay, J. Malanik, and A. P. Barrett, 2012: The Arctic's rapidly shrinking sea ice cover: A research synthesis. *Climatic Change*, **110**, 1005–1027, doi:10.1007/s10584-011-0101-1.

Tilinina, N., S. K. Gulev, I. Rudeva, and P. Koltermann, 2013: Comparing cyclone life cycle characteristics and their interannual variability in different reanalyses. *J. Climate*, **26**, 6419–6438, doi:10.1175/JCLI-D-12-00777.1.

——, ——, and D. H. Bromwich, 2014: New view of arctic cyclone activity from the arctic system reanalysis. *Geophys. Res. Lett.*, **41**, 1766–1772, doi:10.1002/2013GL058924.

Trenberth, K. E., 1997: Using atmospheric budgets as a constraint on surface fluxes. *J. Climate*, **10**, 2796–2809, doi:10.1175/1520-0442(1997)010<2796:UABAAC>2.0.CO;2.

——, J. T. Fasullo, and J. Mackaro, 2011: Atmospheric moisture transports from ocean to land and global energy flows in reanalyses. *J. Climate*, **24**, 4907–4924, doi:10.1175/2011JCLI4171.1.

Tsukernik, M., D. N. Kindig, and M. C. Serreze, 2007: Characteristics of winter cyclone activity in the northern North Atlantic: Insights from observations and regional modeling. *J. Geophys. Res.*, **112**, D03101, doi:10.1029/2006JD007184.

Woods, C., R. Caballero, and G. Svensson, 2013: Large-scale circulation associated with moisture intrusions into the Arctic during winter. *Geophys. Res. Lett.*, **40**, 4717–4721, doi:10.1002/grl.50912.

Yamanouchi, T., 2011: Early 20th century warming in the Arctic: A review. *Polar Sci.*, **5**, 53–71, doi:10.1016/j.polar.2010.10.002.

Zhang, X., J. He, J. Zhang, I. Polyakov, R. Gerdes, J. Inoue, and P. Wu, 2013: Enhanced poleward moisture transport and amplified northern high-latitude wetting trend. *Nat. Climate Change*, **3**, 47–51, doi:10.1038/nclimate1631.